AD-A063 963 PANAMETRICS INC WALTHAM MASS F/G 21/4
ADVANCED TECHNOLOGY FUEL MASS FLOWMETER.(U)
OCT 78 L C LYNNWORTH, N E PEDERSEN, J L SEGER DAAJ02-76-C-0030
UNCLASSIFIED 138 USARTL-TR-78-45 NL

1 OF 1
ADA
063963

END
DATE
FILMED
3 -79
DDC

USARTL-TR-78-45

(12)

ADVANCED TECHNOLOGY FUEL MASS FLOWMETER

Lawrence C. Lynnworth, Norman E. Pedersen,
John L. Seger, James E. Bradshaw
PANAMETRICS, INC.
221 Crescent Street
Waltham, Mass. 02154

October 1978

Final Report for Period June 1977 - June 1978

Prepared for

APPLIED TECHNOLOGY LABORATORY
U. S. ARMY RESEARCH AND TECHNOLOGY LABORATORIES (AVRADCOM)
Fort Eustis, Va. 23604

APPLIED TECHNOLOGY LABORATORY POSITION STATEMENT

This report provides a solution to the problem of monitoring the mass fuel flow of helicopter gas turbine engines. However, the lack of sufficient testing precludes a complete evaluation of the technique, particularly the density measurement portion. Consequently, the reader is cautioned not to consider the accuracies attained as being those of the complete system. Results of this effort will be integrated with other R&D efforts at the Applied Technology Laboratory and at AVRADCOM to establish research and development programs to improve the applicability of this technique to future Army aircraft subsystems.

Mr. Roger J. Hunthausen of the Aeronautical Systems Division served as project engineer for this effort.

UNCLASSIFIED

SECURITY CLASSIFICATION OF THIS PAGE (When Data Entered)

REPORT DOCUMENTATION PAGE

READ INSTRUCTIONS BEFORE COMPLETING FORM

1. REPORT NUMBER: USARTL-TR-78-45
2. GOVT ACCESSION NO.
3. RECIPIENT'S CATALOG NUMBER
4. TITLE (and Subtitle): ADVANCED TECHNOLOGY FUEL MASS FLOWMETER
5. TYPE OF REPORT & PERIOD COVERED: Final Report, Jun 77 - Jun 78
6. PERFORMING ORG. REPORT NUMBER: 138/Final Report
7. AUTHOR(s): Lawrence C. Lynnworth, Norman E. Pedersen, John L. Seger, James E. Bradshaw
8. CONTRACT OR GRANT NUMBER(s): DAAJ02-76-C-0030
9. PERFORMING ORGANIZATION NAME AND ADDRESS: Panametrics, Inc., 221 Crescent Street, Waltham, Massachusetts 02154
10. PROGRAM ELEMENT, PROJECT, TASK AREA & WORK UNIT NUMBERS: 63209A 1F263209DB38 00 023 EK
11. CONTROLLING OFFICE NAME AND ADDRESS: Applied Technology Laboratory, U.S. Army Research and Technology Laboratories, Fort Eustis, Virginia 23604 (AVRADCOM)
12. REPORT DATE: Oct 78
13. NUMBER OF PAGES: 52
14. MONITORING AGENCY NAME & ADDRESS (if different from Controlling Office): 53 p.
15. SECURITY CLASS. (of this report): UNCLASSIFIED
15a. DECLASSIFICATION/DOWNGRADING SCHEDULE

16. DISTRIBUTION STATEMENT (of this Report)

Approved for public release; distribution unlimited.

17. DISTRIBUTION STATEMENT (of the abstract entered in Block 20, if different from Report)

18. SUPPLEMENTARY NOTES

19. KEY WORDS (Continue on reverse side if necessary and identify by block number)

Ultrasonics, mass flowmeter, flow velocimeter, area-averaging, fuel flowmeter

20. ABSTRACT (Continue on reverse side if necessary and identify by block number)

The fuel mass flowmeter system demonstrated in a previous Army program, consisting of an ultrasonic flow velocimeter and a capacitance-type densitometer, was adapted to T-700 gas turbine engine requirements. Mechanical adaptations included the reduction in size and weight of the flow cell to fit the configuration and mounting constraints of a T-700 engine. Electronic developments included repackaging into a portable field-type case, configuration switching and digital delay equalizers, and the (cont'd)

DD FORM 1 JAN 73 1473 EDITION OF 1 NOV 65 IS OBSOLETE

UNCLASSIFIED

SECURITY CLASSIFICATION OF THIS PAGE (When Data Entered)

403 420

mt

UNCLASSIFIED

SECURITY CLASSIFICATION OF THIS PAGE(When Data Entered)

substitution of a microprocessor for a previously used calculator chip, resulting in a choice of response times, or integration times, selectable from ~50s down to ~0.5s. Test results are presented for 7024 Type IIB calibrating fluid over the mass flow rate range $\dot{M}$ = 40 to 1200 PPH, for temperature near 70°F (21°C), and for pressures up to 1500 psig. Performance of the system is discussed with respect to laminar, transitional, and turbulent flow profiles associated with Reynolds numbers from ~50 to ~50,000 and with respect to geometrical constraints imposed by the T-700 configuration.

UNCLASSIFIED

SECURITY CLASSIFICATION OF THIS PAGE(When Data Entered)

PREFACE

The continuing encouragement of R. Hunthausen, G. W. Hogg and R. Scharpf of the Applied Technology Laboratory (AVRADCOM) is appreciated. Transducer fabrication at Panametrics was assisted by K. A. Fowler and D. R. Patch. Helpful discussions with Dr. E. H. Carnevale were conducted throughout the program. K. E. McFarland drafted the line drawings. The excellent cooperation of GE personnel is sincerely appreciated, particularly L. Zirin, P. Capone, J. Jacobson, D. Hebert and S. Wervickas. The cooperation of D. E. Stuart of Simmonds Precision, concerning their densitometer, is acknowledged. The contributions to the mock-ups by B. Marcheterre of Santin Engineering are also acknowledged.

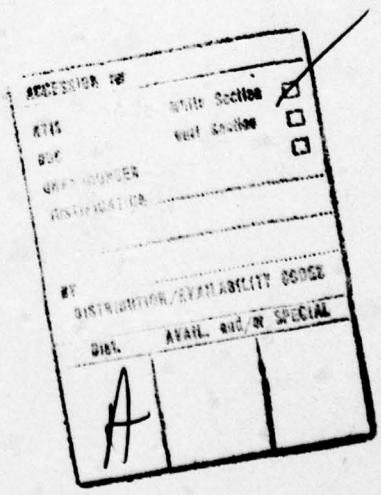

TABLE OF CONTENTS

Section	Page
PREFACE	3
LIST OF ILLUSTRATIONS	6
LIST OF TABLES	7
INTRODUCTION	8
THEORY OF OPERATION	9
FABRICATION	13
TEST RESULTS	18
CONCLUSIONS	26
RECOMMENDATIONS	27
REFERENCES	28
LIST OF SYMBOLS	52

LIST OF ILLUSTRATIONS

Figure		Page
1	Block diagram of 5 MHz "Eustis" system	29
2	Field-type case	30
3	μ processor	31
4	Eustis flow velocimeter for T-700 application	32
5	Transmitter board	33
6	Clock and timing board	34
7	Zero crossing detector board	35
8	Counter board	36
9	Densitometer circuit board	37
10	Fuel mass flowmeter cell fabricated of SS 316	38
11	Flow cell outline dimensions	39
12	Aluminum flow cell model, and components	40
13	Photo of $\dot{M}$ cell mounted on T-700 engine	41
14	End view of $\dot{M}$ cell mounted on T-700 engine	42
15	Tilted top view of M cell mounted on T-700 engine	43
16	Schematic of hydrostatic pressure test conducted April 1977	44
17	ΔP versus M	45
18	Bent tube used in ΔP tests	46
19	Transparent flow cell to test if screens trap vapor bubbles (e.g., air bubbles in water)	47

LIST OF ILLUSTRATIONS (cont'd)

Figure		Page
20	Acrylic cells	48
21	Densitometer calibration from Reference 2	49
22	Low-pressure test loop	50
23	High-pressure test loop	50
24	Calibrating fluid test results	51

LIST OF TABLES

Table		Page
1	Min. and max. values of selected parameters	10
2	Hydraulic, cell, electronic and transducer parameters.	10
3	Pressure drop tests at M = 1000 PPH	21
4	Pressure test: <V> as a function of P	21
5	Hysteresis test: increasing vs decreasing flow	22
6	Calibration test results, 40 to 1200 PPH	23
7	Deviations vs mass flow rate	24
8	Comparison of SOW tests and performance to those attained in the contract	25

INTRODUCTION

The purpose of this program was to adapt the general concept of a fuel mass flowmeter as developed and demonstrated in a previous contract to the configuration, flow rate, and other requirements of a T-700 gas turbine engine installation.

The general concept that provided the basis for the present work was reported by Pedersen, Lynnworth and Bradshaw in 1975 (Reference 1). Basically, the fuel mass flow rate $\dot{M}$ is determined from the equation

$$\dot{M} = \rho V A \qquad (1)$$

where ρ = density, V = flow velocity, and A = cross sectional area of the flow cell duct. ρ is determined from the fuel's dielectric constant, using a Simmonds Precision capacitance densitometer. V is determined ultrasonically, using contrapropagating sequential transmissions of 5 MHz bursts. A is measured by conventional means.

In the present work, the flow cell was reduced in length from over ~ 24 inches (600 mm) down to 4 inches (100 mm) + hydraulic connectors; in weight from ~ 15 lb (6.8 kg) down to 2 lb (0.9 kg) in stainless steel, and potentially down to less than 1 lb (0.45 kg) in aluminum. The electronics system was improved and repackaged to fit in a portable field case having outside dimensions of 14 x 21 x 16 inches (360 x 525 x 400 mm) and weighing 57 lb (26 kg) including all electronics.

---

1. Pedersen, N. E., Lynnworth, L. C., and Bradshaw, J. E., Improved Ultrasonic Fuel Mass Flowmeter for Army Aircraft Engine Diagnostics, Panametrics, Inc.; USAAMRDL Technical Report 75-8, Eustis Directorate, U. S. Army Air Mobility Research and Development Laboratory, Fort Eustis, Virginia, June 1975, AD A013408.

THEORY OF OPERATION

A. Flow Velocimeter Electronics

A block diagram of the fully coherent electronic system that measured $T_1 - T_2$ and T_1 and T_2 is shown in Figure 1. Flow-related parameters are measured by using a fully coherent electronic system that operates synchronously from a 5 MHz crystal-controlled oscillator. The transmitted waveform is generated by means of synchronously gating the output of the 5 MHz oscillator for a 25 to 50 μs interval at a 2 kHz repetition rate (per transducer). Upstream and downstream common-path transmissions are consecutive and spaced 250 μs apart. Independent measurements are made of the phase difference between the upstream and downstream 5 MHz spectral components of the received waveforms and the phase sum of the 2 kHz modulation components of these waveforms. These two independent measurements are combined to yield the Mach number V/c and V, where V = flow velocity and c = sound speed. A high signal-to-noise ratio is achieved by means of narrowband receivers and fully coherent detection, thereby providing distinct advantages in precision and stability over conventional flowmetering techniques, which utilize broadband pulses. In the previous Eustis program (Reference 1) this type of system provided a precision of ~ 1/4 percent full scale (FS). Its principles of operation, and test data for laminar, transitional, and turbulent flow, for different fuels and fuel temperatures from 10 to 46°C, are given in detail in Reference 1.

It is shown in Reference 1 that, since the upstream minus downstream transit time (or phase) is proportional to V/c^2, the flow velocity V is obtainable from

$$V = k(T_1 - T_2)/T_1T_2 \qquad (2)$$

where k = constant.

B. Flow Velocimeter Acoustics and Hydrodynamics

The flow cell was designed to provide area-averaging on the flow profile despite laminar, transitional, and turbulent flow regimes (Table 1), despite unfavorable (nonideal) inlet conditions, and without the use of flow straighteners or a static mixer. At the outset of this program, and throughout its course, the only practical cell concept for which published

TABLE 1. MINIMUM AND MAXIMUM VALUES OF SELECTED PARAMETERS.

Parameter	Units	Minimum	Maximum
P	psia	14.7	(dynamic); 1500 (static)
T	^{o}F	-65	(ambient); 300 (fuel)
	^{o}C	-54	74 149
$\dot{M}$	PPH	100	1,000
	g/s	12.63	126.3
ρ	g/cm^3	0.65	0.90
$\overline{V}$	cm/s	8.7	120
ν	stokes	0.003	0.30
Re	-	37	51,000
c	m/s	750	1,700
Δt	ns	0.77	54
$\Delta\phi$	deg	1.4	97

TABLE 2. HYDRAULIC, ELECTRONIC, CELL, AND TRANSDUCER PARAMETERS.

Item	Description
Hydr. connectors	AN -3 and -4 sizes
Carrier frequency	5 MHz
Pulse repetition frequency	2 kHz
Pulse width	25μs
Bandwidth: 1st 1F detector	700 Hz
2nd 1F detector	~100 Hz
V duct area	Square, 0.505 x 0.505 in. (1.28 x 1.28 mm)
L	1.01 inch (2.56 cm)
Transducer material	K81 lead metaniobate type
Cell weight	2 lb (0.9 kg) in SS 316 0.7 lb (0.3 kg) in Al
Cell envelope dimensions	2 x 2 x 4 in. (5 x 5 x 10 cm) + connectors

data supports the area-averaging objective is the rectangular concept demonstrated in Reference 1. This concept combines a rectangular flow duct in which the flow is interrogated obliquely at 45° over the entire flow cross section. To the extent that flow is axial and the acoustic beam is plane and uniform, equal area segments of fluid are weighted equally. This is the basis for proper area-averaging despite profile uncertainties. In other words, to the extent that the stated conditions prevail, $V \equiv \overline{V}$.

C. Fuel Densitometer

The relationships between density ρ and dielectric constant ϵ for aviation fuels have been developed since the 1950's. The hydrocarbons in aircraft fuels are nonpolar liquids. For a nonpolar liquid, a theoretical relationship between dielectric constant and density is the Clausius-Mosotti law (See Reference 2 and Figure 21):

$$(\epsilon - 1)/(\epsilon + 2) = C\rho \qquad (3)$$

where C = polarizability. This relationship is rearranged and called the "fuel regression line" in capacitance fuel-gaging literature. One fuel regression line is

$$(\epsilon - 1)/\rho = b + a(\epsilon - 1) \qquad (4)$$

where a and b are constants.

The polarizability C varies only slightly from one hydrocarbon to another hydrocarbon for the principal constituents of aircraft fuels. Thus, the dielectric constant, as expressed by the Clausius-Mosotti law, is a good measure of fuel density.

Figure 4 in Reference 2 is a plot of density versus dielectric constant for some typical samples of JP-4. This figure illustrates what is commonly called "fuel error". This fuel error is the deviation of a given sample from the theoretical best average straight line, which is called the "JP-4 line of regression".

Further statistical analysis of this and also JP-5 data is plotted in Figure 5 of Reference 2. The interpretation of this plot is that 95.5 percent of the samples measured (JP-4 and JP-5) fall within 1.3 percent of the JP-4 line of regression. From these data it is thus possible to

---

2. Stuart, Douglas E., Flow: Its Measurement and Control in Science and Industry, Proceedings of May 1971 ISA Symposium, Volume 1, Part 2, Pennsylvania, 1974, pp. 687-693.

predict a 2σ error of 1.3 percent or less. The data have been further analyzed and 1σ and 3σ errors are included. (Here, σ = standard deviation.) The cited Figures 4 and 5 are combined in Figure 21.

For normal commercial fuels, more recent data collected by Air Canada and United Air Lines show that of 55 samples, 51 are within $\pm$ 1 percent of variation from the JP-4 line. This tends to confirm the previous prediction.

Note that the Clausius-Mosotti law is nonlinear. However, the nonlinearity is only 0.5 percent at the densities corresponding to fuels at +160°F and -50°F (71°C and -46°C).

D. Mass Flow Rate

The mass flow rate $\dot{M}$ is given by Equation (1), $\dot{M} = \rho VA$, where V is now interpreted as $\overline{V}$. The electronics digitally multiplies the ρ and V inputs, and digitally scales the product to account for the cell dimensions (area A, and axial path length L; see Table 2). $\dot{M}$ is thus available for display and for recording, with a response time selectable according to the number of interrogations (data points) to be averaged.

The volumetric flow rate equals VA. The totalized volumetric flow equals the integral of V(t) A dt, integrated for the time interval t. The totalized mass equals the integral of $\dot{M}$ dt.

Of historic interest, one may note that attempts to measure fuel $\dot{M}$ ultrasonically were reported by Kritz as early as 1955 (Reference 3). However, both Kritz's early work, and Roth's subsequent work using a different ultrasonic approach, were abandoned (Reference 4). In the early 1970's Panametrics conducted ultrasonic experiments on configurations that were similar in principle to Kritz's (Reference 5). But in 1975 it was decided to measure only V ultrasonically (by our rf burst method), and ρ dielectrically (Reference 1). When new ultrasonic densitometers or velocimeters become available, these ρ and V decisions may be revised.

---

3. Kritz, J., ISA Proc. 10 Part 2, 55-16-3, pp. 1-6 (1955); Instruments and Automation 28, 1912-1913 (Nov. 1955); J. L. McShane, pp. 897-913, in Ref. 2.
4. Roth, W., U.S. Patent No. 3,188,862 (June 15, 1965).
5. Lynnworth, L. C., and Pedersen, N. E., USAAMRDL TR 72-66 (Jan. 1973); Proc. IEEE Ultrasonics Symp. 81-84 (1972), IEEE Cat. No. 72 CHO 708-8 SU.

FABRICATION

A. Electronics

Figures 2 through 9 illustrate the electronic portion of the $\dot{M}$ system fabricated in this program. All the electronics is housed within the metal field-type case shown in Figure 2. The electronics incorporated in this system, although the same in principle as in the previous contract, is considerably more sophisticated. The main improvement has been to provide "configuration switching", which in effect periodically reverses the outputs of the two 5 MHz filters so that the following computation can be made by the microprocessor:

$$\overline{\Delta\phi} = \frac{1}{2} (\Delta\phi_A + \Delta\phi_B) \qquad (5)$$

where $\overline{\Delta\phi}$ is the average phase difference between the upstream and downstream 5 MHz components of the received signals, $\Delta\phi_A$ is the phase difference in the "A" filter configuration and $\Delta\phi_B$ refers to the reversed, or the "B" configuration.

The previously used hard wire calculator chip has been replaced by a programmed prolog microcomputer utilizing an 8080 cpu chip.

Individual circuit boards and the microprocessor are shown in Figures 3 through 9. The principal differences between the electronics fabricated in this program and those in the previous program may be explained as follows:

1. A programmable microcomputer is incorporated in the present system, rather than the hard wire programmed calculator chip of the previous program. The microcomputer utilizes 1K and 3K bytes of random access memory and read-only-memory, respectively. These can conveniently be doubled, should future requirements show the need for it.

   Although a calculator chip was utilized during the previous contract, this was only a first primitive step, as compared with the presently used microcomputer. The microcomputer (manufactured by Prolog) is much faster than the calculator chip, by

more than two orders of magnitude, which eliminates the lower limit of 5 seconds on system response time. In addition, the microprocessor software has been prepared so as to accept the ΔT inputs from the counter circuits in both the normal and reversed filter configurations and to sum these, thereby eliminating the effects of filter drift (note that this was done manually during the previous contract).

2. Configuration switching has been built into the present system, but was absent in the previous system. The result of this is to cancel the effects of phase shifts and variations of them in the 5 MHz and the 2 kHz filters of the electronics portion of the velocimeter.

3. Improved zero-cross detectors have been designed, tested, and incorporated in the present system. These are essentially immune to ambient temperature effects and have improved the overall stability of the system, as compared with the previous system.

4. Digital delay equalizers (as compared with analog equalizers in the previous system) have been included in the present system to provide zero-phase adjustment between the two filter channels. This feature improves overall stability.

5. Minimum response time has been reduced from 12 seconds to 0.5 second. The response time is adjustable at the front panel. This allows for a trade-off between statistical flow-dependent fluctuations and system response time.

   The system response time is adjustable up to 49.5 seconds in 0.5 second increments, via a front panel thumbwheel switch.

   It is possible, by increasing response time, to reduce the statistical fluctuations in the output due to turbulent flow fluctuations. The improvement in output repeatability is proportional to the square root of the increase in response time. This improvement has been observed in our laboratory tests at Panametrics.

   Considerable difficulties were encountered in the electronics. These problems were mainly due to feedthrough in the solid-state switches used for transmitter/receiver isolation and for configuration switching. Since the system is coherent, it is very

immune to extraneous external signals, but (by the same token) it is quite sensitive to its own internally generated signals, which are derived from the 5 MHz clock. Extensive work was done to shield the sensitive receiver section from internal pickup. However, a residual false signal level due to feedthrough persists and results in a zero offset of about 0.5 ft/sec. Since this is a constant of the system, it can be eliminated during calibration.

B. Flow Cell

The deliverable flow cell fabricated in this program is shown in Figure 10. The body was made of SS 316. This material was selected for weldability, corrosion resistance, strength, and to assure acoustic isolation between transmitter and receiver transducers.

Although it was known at the outset that Al or Ti alloys, if used for the flow cell body, could certainly reduce weight, the transducer design that was available required SS for the cell in order to assure acoustic isolation. However, if the transducers could be isolated from the cell, then the ultrasonic attenuation coefficient in the cell material no longer needs to be high.

At the end of the program (see next paragraph) a new transducer design emerged that provided the desired isolation, as an unexpected benefit associated with its thin shim window. The Al flow cell mock-up of Figure 12 was rebored to accommodate this new transducer design, and to facilitate laboratory testing of the flow velocimeter using water. These tests demonstrated that the acoustic isolation of the new transducers was adequate to enable Al to be used as the cell body material. Thus, in the future, the flow cell of the present configuration could be built largely of Al, resulting in a total cell weight of less than 1 lb (< 0.5 kg).

The details of the ultrasonic components investigated in the program for use with this cell are shown in the exploded view of Figure 12. The Al model shown in this photo was originally fabricated to establish machining sequences, to verify fabricability, and to check configuration compatibility on a T-700 engine (see Figures 13-15). The Ti window was replaced late in the program with a stainless steel shim. The graphite backing was simplified to a rectangular block, and the Teflon insulator was replaced with a thermalloy sheet. The square-holed sleeve, of SS 316, was electron beam (EB) welded to the fuel inlet transition and, as in the previous program, its transducer ports were screened to reduce the tendency to

generate eddies. The square-holed sleeve is broached to produce a duct cross section with dimensions of 0.505 x 0.505 inch (12.8 x 12.8 mm). The 45° obliquely incident 5 MHz beam can thus be reflected along the desired interrogation path.

The Simmonds Precision densitometer has been installed on the following aircraft:

Grumman EA-6B flight test aircraft
Grumman KA-6D tanker/150 systems delivered
Cessna 500 Citation/600 systems delivered
Grumman F-14 A and B flight test aircraft/40 systems delivered.

Accordingly, this system is considered to be a well-established method of accurately determining the density of widely varying jet fuels in dynamic situations.

In a region generally parallel to the V part of the flow cell, a capacitance densitometer element measures the dielectric constant of the fuel as it passes through the element, thereby accomplishing system density compensation. The plates of the capacitance compensator unit are three concentric metal tubes, SS316, insulated from each other and from the flow cell housing. The outer and inner tubes are guard, or low-impedance elements, and the center tube is the high-impedance plate. An energizing field is applied to the compensator by a precision audio frequency oscillator. Changes in fuel dielectric constant create varying signal currents, which are then amplified and conditioned into a signal that is proportional to density variations. For safety, the energizing current is limited to a maximum of 10 mA under worst-case circuit failure conditions.

Two shielded conductors run from the flow cell to the M electronics. The densitometer electronic circuit board is hard wired to meet vibration specifications.

In order to arrive at an acceptable design that fits the flow cell to the T-700 configuration, a sequence of wooden mock-ups were fabricated. These mock-ups embodied numerous suggestions of L. Zirin and P. Capone of GE, and B. Marcheterre of Santin Engineering

For completeness, it should be stated that at one of the first cell design meetings a few of our flow cell design alternatives that had already been fabricated (but not yet tested thoroughly) were brought to GE's attention. In general, our industrial-grade flow cell weldments were too large and too heavy for consideration. However, one design, using small-diameter

tubing (~ 9 mm OD) and standard compression fittings, was judged desirable from the point of view of size and weight. However, at that time, the "small tube" flow velocimeter could not provide mass flow rate, since the capacitance densitometer required an internal volume on the order of 1 inch diam x 3 inches long (25.4 mm diam x 75 mm long). In addition, its area-averaging was unproven. Accordingly, after a series of mock-up iterations, the final cell design evolved (Figures 13-15).

The present contract did not require that a practical mount be developed. However, to show the general design of such a mount, and to show that the final cell design could indeed be fitted to a T-700 engine, a sheet-metal mount was fabricated and is shown in Figures 13 through 15.

The total cell can be installed or removed without any additional or special tools. This result was achieved by utilizing an existing flange lip to secure the flow cell mount with the same type of screw fasteners as are ordinarily used at this location. Also, the same -3 and -4 AN fitting sizes are used elsewhere on the T-700 engine.

TEST RESULTS

A. Pressure Tests

1. Hydrostatic Pressure Tests

Hydrostatic tests were conducted using water at zero flow at Artisan Industries, Waltham, Massachusetts on 12 April 1977, using the setup shown in Figure 16. The cell was cycled 10 times from ~ 0 to 1500 psig and no leaks were observed. In this test the transducer design included the Ti window, 0.237 inch (6 mm) thick.

Subsequently the Ti window was replaced with a 0.002-inch-thick (0.05 mm) SS shim. Two transducers containing this thin shim window were installed in the modified (rebored) SS 316 cell body and tested again to 1500 psig. This test was conducted at GE-Lynn in March 1978, using the 7024 calibrating fluid. Pressure was applied for several minutes. No leaks were observed. Accordingly, the cell was deemed suitable for installation in the test stand, and preliminary dynamic pressure tests commenced. At $\dot{M}$ = 1000 PPH, ΔP did not exceed 50 psig.

2. Dynamic Pressure Tests at GE, June 1978

Three types of dynamic pressure tests were conducted at GE-Lynn on 23 June 1978. First, the pressure drop ΔP was measured as a function of $\dot{M}$, and found to be nearly proportional to $\dot{M}$, up to 1000 PPH (Figure 17). Second, ΔP was measured at $\dot{M}$ = 1000 PPH for four different U-turn configurations between inlet and outlet (Table 3). Third, the influence of P on the indicated V was determined at $\dot{M}$ = 1000 PPH (Table 4). At 1000 PPH, $\Delta P \approx 40$ psi.

From Table 3, it is seen that the basic design has lower ΔP than a comparable length of -3 size flexible hose, or a comparable length of bent tubing (Figure 18). The "enlarged" U-turn referred to in Table 3 reduced ΔP by only 2 psig, or 5%. Thus, the main contributions to ΔP are losses due to the -3 and -4 fittings.

In the present design, the selection of -3 and -4 sizes is based on GE's recommendation, which in turn is based on configuration compatibility. However, for cases where larger fittings could be utilized, the basic duct geometry, despite the U-turn, would generate a much lower ΔP.

Referring now to Table 4, the $<V>$ data show some scatter as P increased, but there is no systematic trend. Therefore, it appears that no P dependence is exhibited. However, acoustic noise was observed to increase at higher P.

B. Hysteresis Test

Table 5 compares average flow velocity data on increasing versus decreasing flow. For most of the points, the difference in readings expressed in terms of full scale (FS) is 1% or less. The standard deviation, σ, is 0.47%.

C. Calibration Test

Calibration data obtained at GE-Lynn on 23 June is tabulated in Tables 6 and 7. As noted in Table 6, each $<V>$ number is the arithmetic average of five readings of five data sets. Thus, for flow conditions in which jitter or noise causes scatter in the five sets, σ is larger. For example, σ = 27 counts at 1200 PPH, but $\sigma < 6$ counts for all M below 1000 PPH. Between 100 and 1000 PPH, the $\sigma / <V>$ values are, with one exception, less than 2% of point, and generally better than 1% FS.

It was planned to measure ρ in these tests, and multiply ρ by V and then by a constant K, to compute $\dot{M}$. The SP densitometer is suitable for JP-4 or JP-5, and also for the calibrating fluid, which is very similar to JP-4. Unfortunately, on 23 June, a malfunction in the ρ system occurred, preventing ρ from being measured in these particular runs.

As it turned out, the available test stand was operated at nearly constant temperature during all tests. Therefore ρ is taken as 0.76 g/cm^3, constant for all tests on 23 June. Using this value, Table 7 presents the linearity as a function of $\dot{M}$, by forming the ratio $R = <V> / \dot{M}$. It is seen that the average value of this ratio is $<R> = 0.447$. The percentage difference ΔR between R at any $\dot{M}$ and $<R>$ is listed in Table 7. Figure 24 presents the corresponding data, up to the contractual M of 1000 PPH.

Table 8 compares the statement of work (SOW) tests and performance to those attained in the contract.

D. Vibration Test

Vibration tests were not performed because of schedule constraints. All components most likely to be sensitive to vibration, such as transducers or the screen, were tested in the previous contract and showed no degradation due to vibration. Therefore, no vibration problems are expected with the present design.

E. Transducer Temperature Exposure Tests

An epoxy-bonded transducer of the type used in the flow calibration tests was tested, exposed to +250°F (+121°C) for 1 hr, and then retested while cooling towards room temperature. The test consisted of measuring the normal-incidence echo amplitude from a reflector submerged in water. Similarly, cold tests were conducted before and after 1 hr exposures to -75°F (-59°C). No change in echo amplitude was observed in either the hot or cold exposure test.

It may be noted that bonding agents are available with temperature capabilities beyond the levels tested above. Such agents include high temperature epoxy adhesive, solder, glass frit, ceramic-base cements, thermal diffusion bonding alloys, etc. Depending on the environment to be withstood, the transducer material, ultrasonic frequency and other considerations, an optimum bonding agent may be selected.

TABLE 3. PRESSURE DROP TESTS AT M = 1000 PPH, 79°F, INLET PRESSURE = 75 psig.

U-turn style	ΔP, psig	Notes
NPT	40	1
Enlarged	38	2
Bent tube	43	3
Flex hose	48	4

(1) Basic design: 1/8" NPT tap drill connects ρ and V parts; NPT plug seals end of cell.

(2) Connection between ρ and V parts enlarged using 3/4" diameter end mill; end welded shut using plate with vanes.

(3) Bent tube illustrated in Figure 18; 3/16" ID x 5.5" long.

(4) Flexible hose length approximately 1 ft.

TABLE 4. PRESSURE TEST: COMPARISON OF <V> AS A FUNCTION OF P, AT $\dot{M}$ = 1000 PPH.

	Inlet pressure, psig	T, °F	<V>, counts
	100	72	483
	300	74	483
	500	77	471
	700	80	493
Average <V>			483
σ			9
σ/<V>, %			1.9

TABLE 5. HYSTERESIS TEST: COMPARISON OF CALIBRATION DATA FOR INCREASING VERSUS DECREASING FLOW. 23 JUNE 1978.

M PPH	<V>, Counts Incr	Decr	Differences Counts	% Point	% Full Scale
40	17.6	14.9	2.7	17	0.6
80	36.6	37.8	-1.2	-3.2	-0.3
100	44.4	48.4	-4.0	-8.6	-0.8
200	79.6	85.5	-5.9	-7.1	-1.2
400	182	175	7	3.9	1.5
600	264	270	-6	-2.2	-1.3
800	363	368	-5	-1.4	-1.0
1000	476	477	-1	-0.2	-0.2
Average %FS Difference					0.86

TABLE 6. CALIBRATION TEST RESULTS FOR FLOW VELOCIMETER ON GE-LYNN WHITELY TEST STAND, 7024 TYPE II CALIBRATING FLUID, T = 72 ± 2°F, INLET PRESSURE = 74 psig ATM = 1000 PPH, ΔP = 40 psig at $\dot{M}$ = 1000 PPH. DATE OF TEST: 23 JUNE 1978. ROTAMETER ACCURACY ± 1/2% OF READING. $\langle V \rangle_{1000}$ = 476.5.

$\dot{M}$ PPH	$\langle V \rangle$ Counts	σ Counts	$\frac{\sigma}{\langle V \rangle}$ %	$\frac{\sigma}{\langle V \rangle_{1000}}$ %
40	17.6	0.62	3.5	0.13
80	36.6	1.43	3.9	0.30
100	44.4	1.40	3.2	0.29
200	79.6	1.61	2.0	0.34
400	182	2.3	1.3	0.48
600	264	2.0	0.7	0.42
800	363	3.7	1.0	0.78
1000	476	5.9	1.2	1.24
1200	544	27	5.0	5.70
1000	477	3.3	0.7	0.69
800	368	3.3	0.9	0.69
600	270	4.7	1.7	0.99
400	175	1.7	1.0	0.36
200	85.5	1.4	1.6	0.29
100	48.4	1.1	2.2	0.23
80	37.8	1.3	3.5	0.27
40	14.9	0.8	5.0	0.17

Notes: $\langle V \rangle$ = average of five readings of five data sets each. σ = standard deviation. $\sigma / \langle V \rangle$ values are percent of point.

TABLE 7. R, ΔR, % POINT AND % FS DEVIATION VERSUS $\dot{M}$, DERIVED FROM TABLE 6.

$\dot{M}$ PPH	$R = \overline{V}/M$ Counts/PPH	$\frac{\Delta R}{\langle R \rangle} \times 100$ % of Point	$\frac{\Delta R}{\langle R \rangle} \frac{V}{V_{max}} \times 100$ % FS
100	0.444	-0.67	-0.05
200	0.398	-10.96	-1.6
400	0.455	-1.79	+0.6
600	0.440	-1.57	-0.76
800	0.454	+1.57	+1.04
1000	0.476	+6.49	+5.68
1200	0.453	+1.34	+1.34
1000	0.477	+6.71	+5.88
800	0.460	+2.91	+1.97
600	0.450	0.67	+0.33
400	0.438	-2.01	-0.65
200	0.428	-4.25	-0.67
100	0.484	+8.28	+0.74
Average	0.447	3.86	1.07
σ	-	3.41	2.31

TABLE 8. COMPARISON OF SOW TESTS AND PERFORMANCE TO THOSE ATTAINED IN THE CONTRACT.

Parameter	SOW	Attained
Design Concept	DAAJ02-73-C-0054	DAAJ02-73-C-0054
Fuel Type	JP-4, JP-5, mixtures	7024 Type II
M Range, PPH	100-1000	40-1000
$\dot{M}$ Overange, PPH	-	1500
Accuracy, % FS	$\pm$ 1/2	$\pm$ 2 } Note: tested at constant ρ; not verified with ρV system.
Hysteresis, % FS	-	$\pm$ 1/2 }
Response Time, s	2	0.5, adjustable to 49.5
Contaminated Fuel	MIL-F-8615C, 4 hr	-
Pressure, psi	1500	1500 static & cyclic; dynamic ΔP vs $\dot{M}$, up to 700 psig
ΔP	No excess	ΔP = 40 psi at $\dot{M}$ = 1000 PPH. This ΔP is less than that in a comparable length bent tube with AN-3, -4 fittings.
Vibration	MIL-STD-810C, Proc. I w/o vibration isolators	-
Fuel Temperature	-65°to +300°F but no-fuel exposure test to 250°F; cal. from 50° to 115°F	Preliminary tests on 7024 up to 140°F; 70°F calibration; transducer tested before and after exposure to -75° and +250°F
Ambient Temperature	-65° to +160°F	
Flow Cell	T-700 configuration	T-700 configuration
Mounting	-	T-700 configuration
Cell Weight	5 lb	2 lb in SS, 1 lb in Al
Electronics	In field-type case	In field-type case. Includes µP; config. switch; digital delay equalizers.

CONCLUSIONS

Based on the observations made and the data recorded in this program, the authors conclude that:

1. The flow cell of Figure 10 satisfies the configuration requirements of a T-700 engine. It can be designed with a mount suitable for easy, rapid installation or replacement. No special tools are required for its installation, maintenance, or repair.

2. The flow cell has no moving parts nor small orifices in the flow path.

3. The flow cell acoustically averages the flow profile despite non-ideal inlet and outlet conditions and despite unknown profiles (laminar, transitional, or turbulent, and ~ 1000:1 Re range, from ~ 50 to ~ 50, 000) in a manner that appears to be superior to any other data-documented method that is applicable to T-700 constraints. As the entire flowing cross section is interrogated, area averaging is inherently better than any point device, with respect to accurate measurements for variable flow conditions. Accuracy of the present flow velocimeter (cell + electronics) appears to be 2% of full scale.

4. In hysteresis tests, precision (1σ) of 0.47 percent of full scale was achieved, with a 30:1 flow range. Over-ranging by a factor of 1.5 produced no damage. This is an advantage over turbine meters, whose bearings are subject to damage at excessive speeds.

5. Pressure drop could be reduced substantially by choosing larger hydraulic fittings for the inlet and outlet.

6. The system can be scaled to measure flow rates that are larger by 1 or more orders of magnitude.

7. Response time could be reduced from the present nominal value of 5 s (for engine diagnostics) to ~ 0.03 s (for engine control). Depending on accuracy/cost trade-offs, the fast response version of this system could utilize either low-cost analog computation or high-accuracy fast digital computation.

RECOMMENDATIONS

Additional tests are recommended, over a wider range of temperature, and with contaminated fuel, and finally, under vibration. These tests should involve the complete system with an operational densitometer.

In view of changing requirements, both for diagnostics and control, the possible utilization of newer, less expensive velocimeter designs should be considered, as well as smaller densitometers that may become available and may be applicable to smaller flow cells.

If the present flow cell design is retained, its body should be fabricated of an aluminum alloy. A T-700 mount appropriate for this reduced-weight cell should be designed, fabricated and tested.

Minor changes in the velocimeter electronics are recommended, to reduce the effects of internal noise or acoustic noise due to pumping at high pressure. These improvements may improve the accuracy of the present approach from ~ 2% to perhaps 1/2% of full scale, or to the limit imposed by the flow cell.

REFERENCES

1. Pedersen, N. E., Lynnworth, L. C., and Bradshaw, J. E., Improved Ultrasonic Fuel Mass Flowmeter for Army Aircraft Engine Diagnostics, Panametrics, Inc.; USAAMRDL Technical Report 75-8, Eustis Directorate, U.S. Army Air Mobility Research and Development Laboratory, Fort Eustis, Virginia, June 1975, AD A013 408.

2. Stuart, Douglas E., Flow: Its Measurement and Control in Science and Industry, Proceedings of May 1971 ISA Symposium, Volume 1, Part 2, Pennsylvania, 1974, pp. 687-693.

3. Kritz, J., ISA Proc. 10 Part 2, 55-16-3, pp. 1-6 (1955); Instruments and Automation 28, 1912-1913 (Nov. 1955); J. L. McShane, pp. 897-913, in Ref. 2.

4. Roth, U.S. Patent No. 3, 188, 862 (June 15, 1965).

5. Lynnworth, L. C., and Pedersen, N. E., USAAMRDL TR 72-66 (Jan. 1973); Proc. IEEE Ultrasonics Symp. 81-84 (1972), IEEE Cat. No. 72 CHO 708-8 SU.

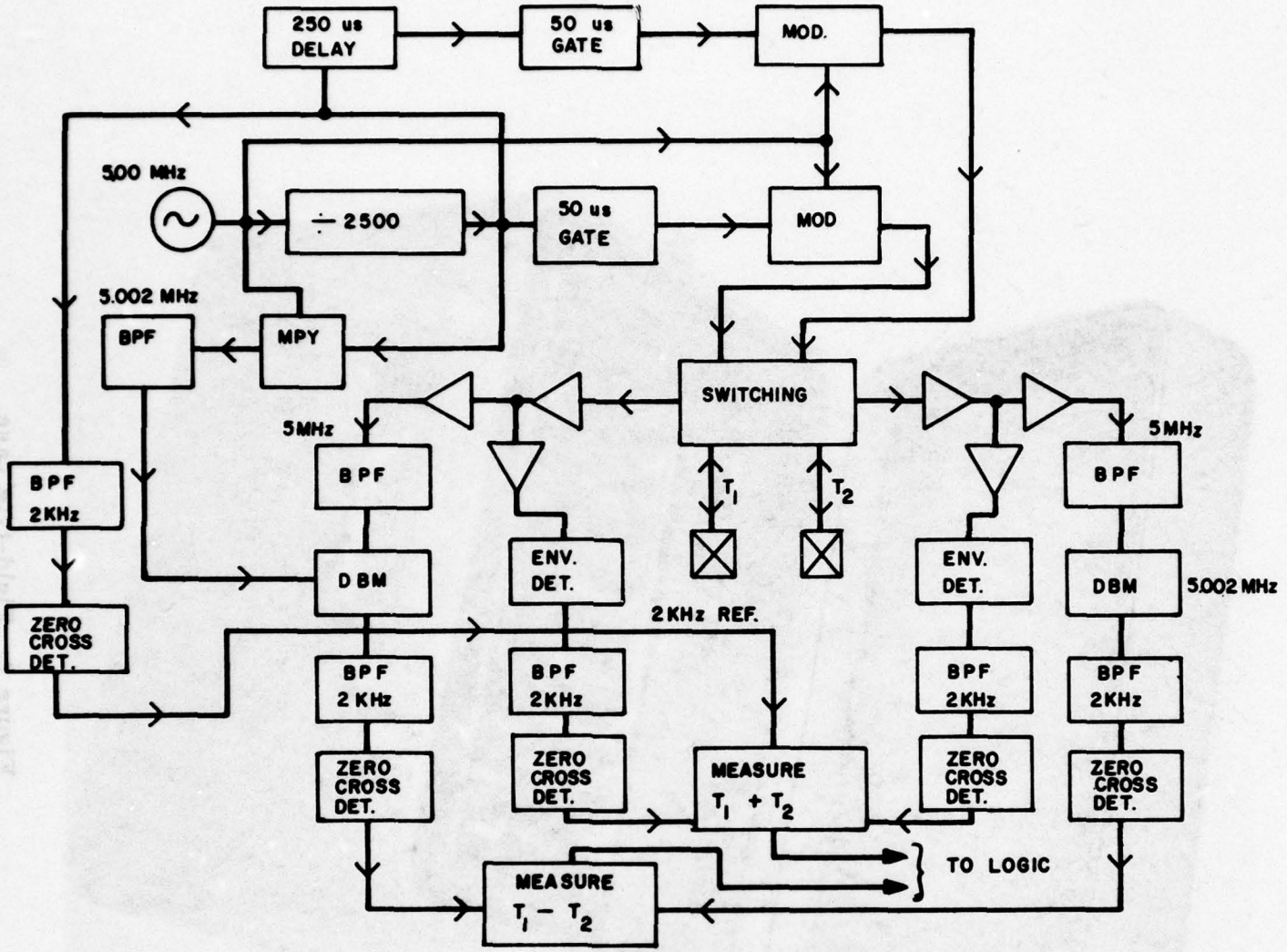

Figure 1. Block diagram of 5 MHz "Eustis" system.

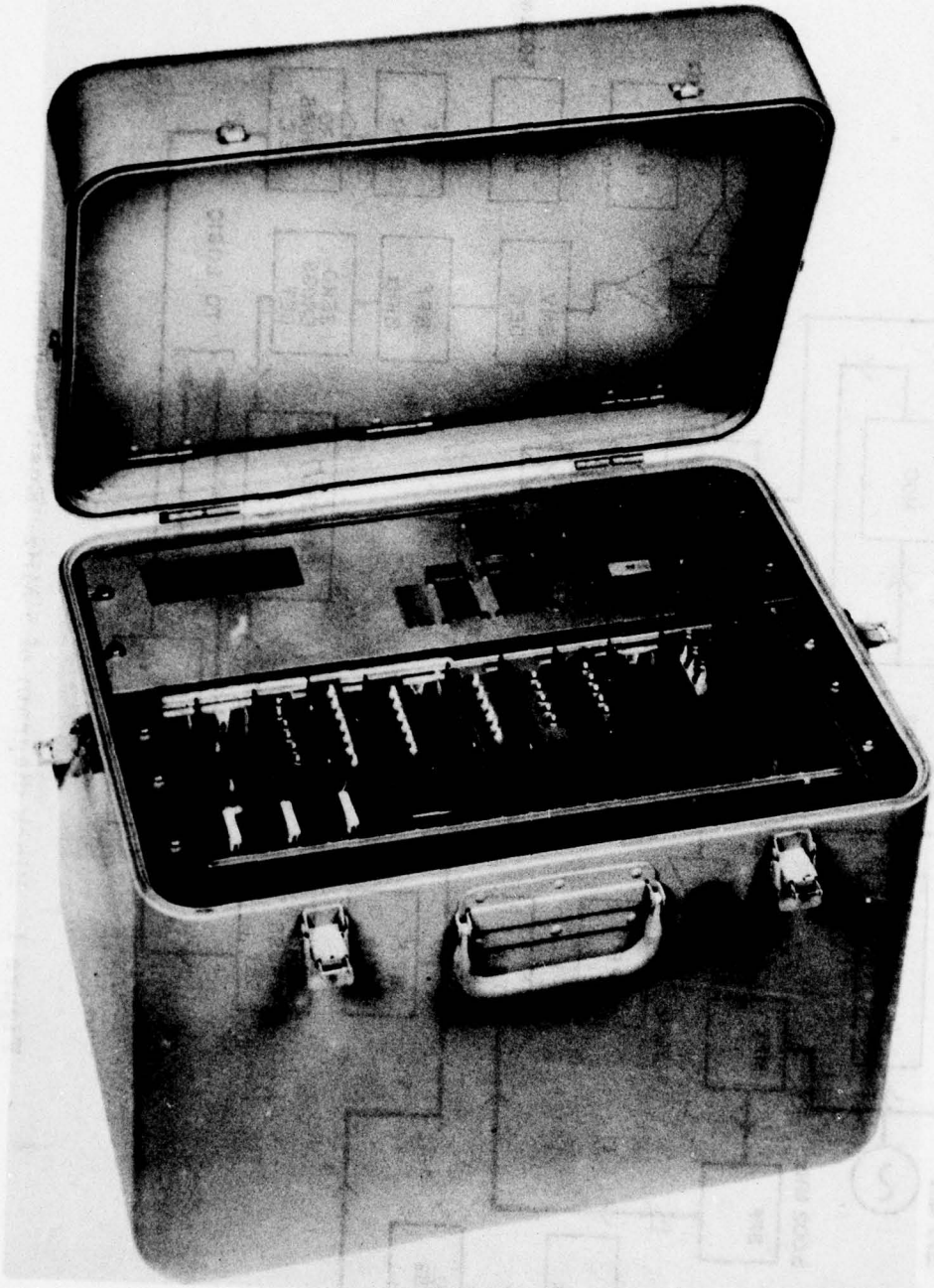

Figure 2. Field-type case.

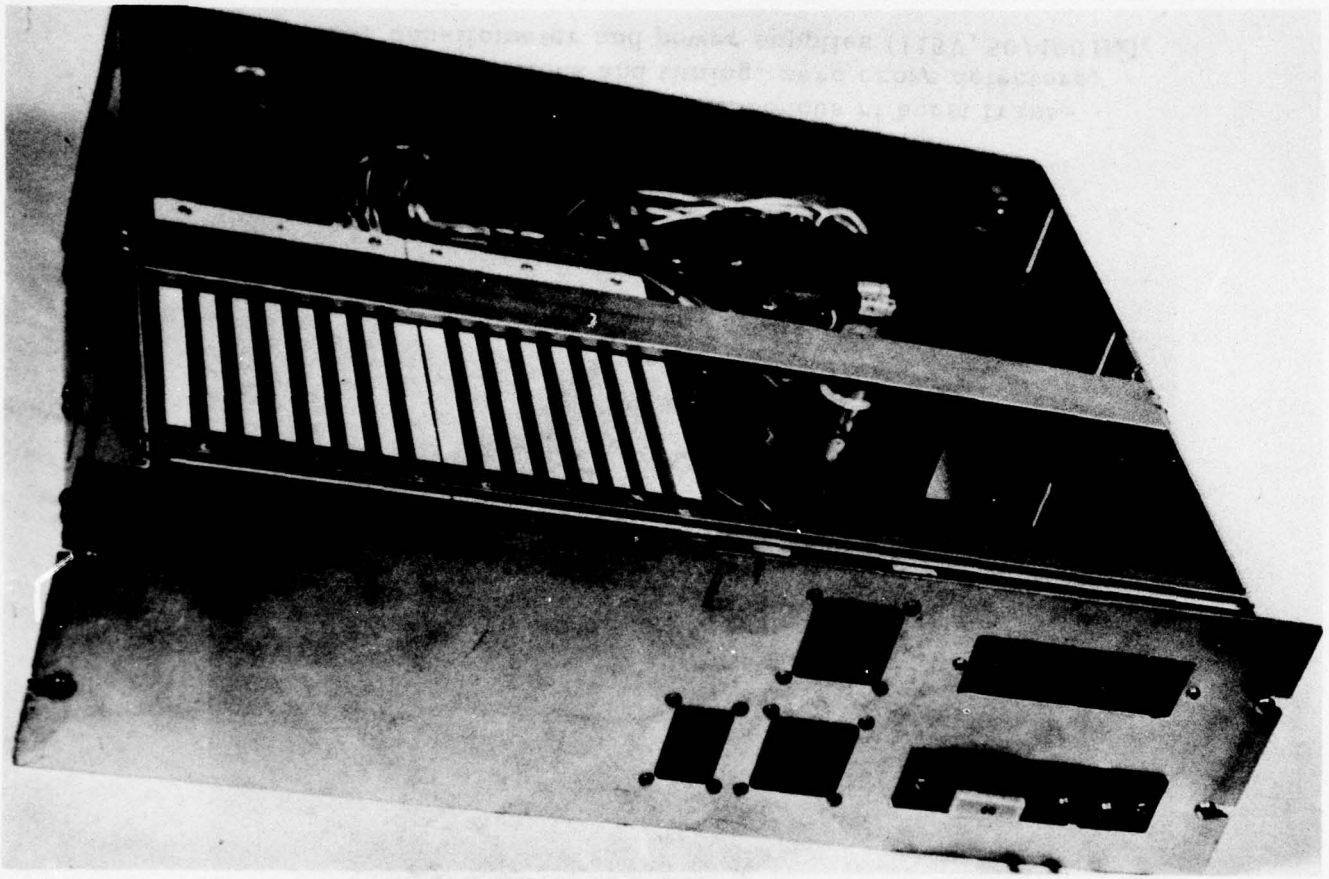

μProcessor makes all M computations and displays average of selected number of measurements.

Figure 3. μProcessor.

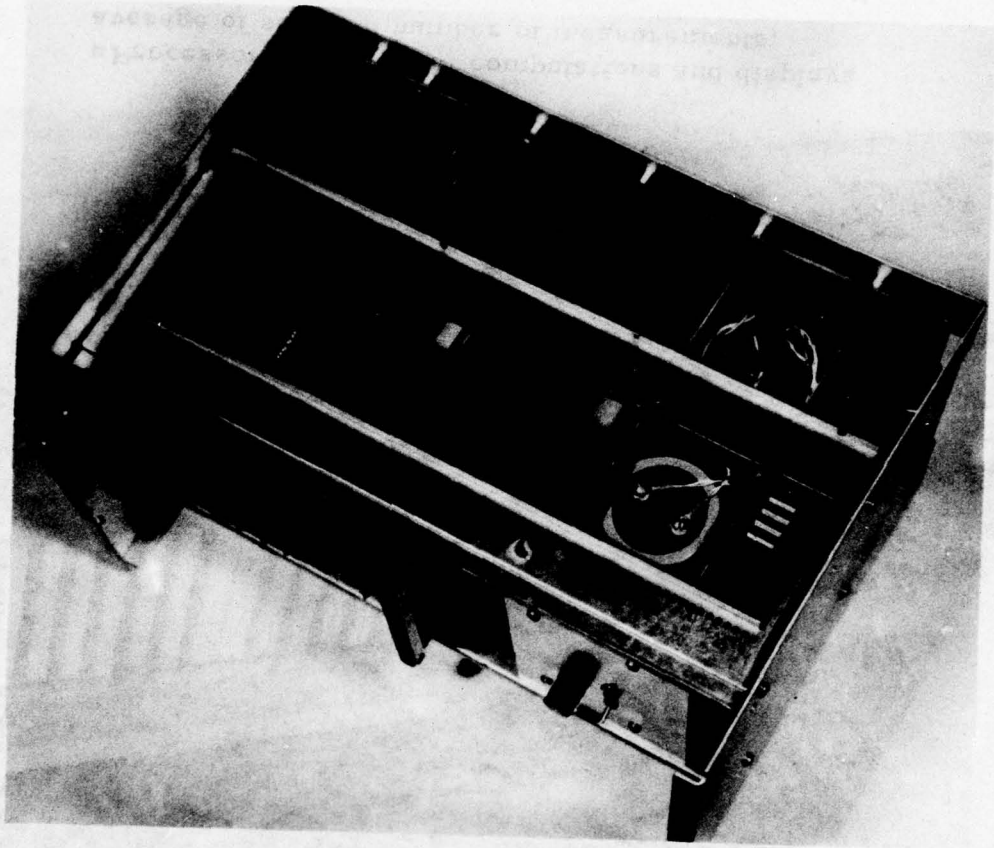

Velocimeter includes 5 MHz synchronous rf burst transmitter, receiver, clock and timing, zero cross detectors, counters, densitometer and power supplies (115V, 50/400 Hz).

Figure 4. Eustis flow velocimeter for T-700 application.

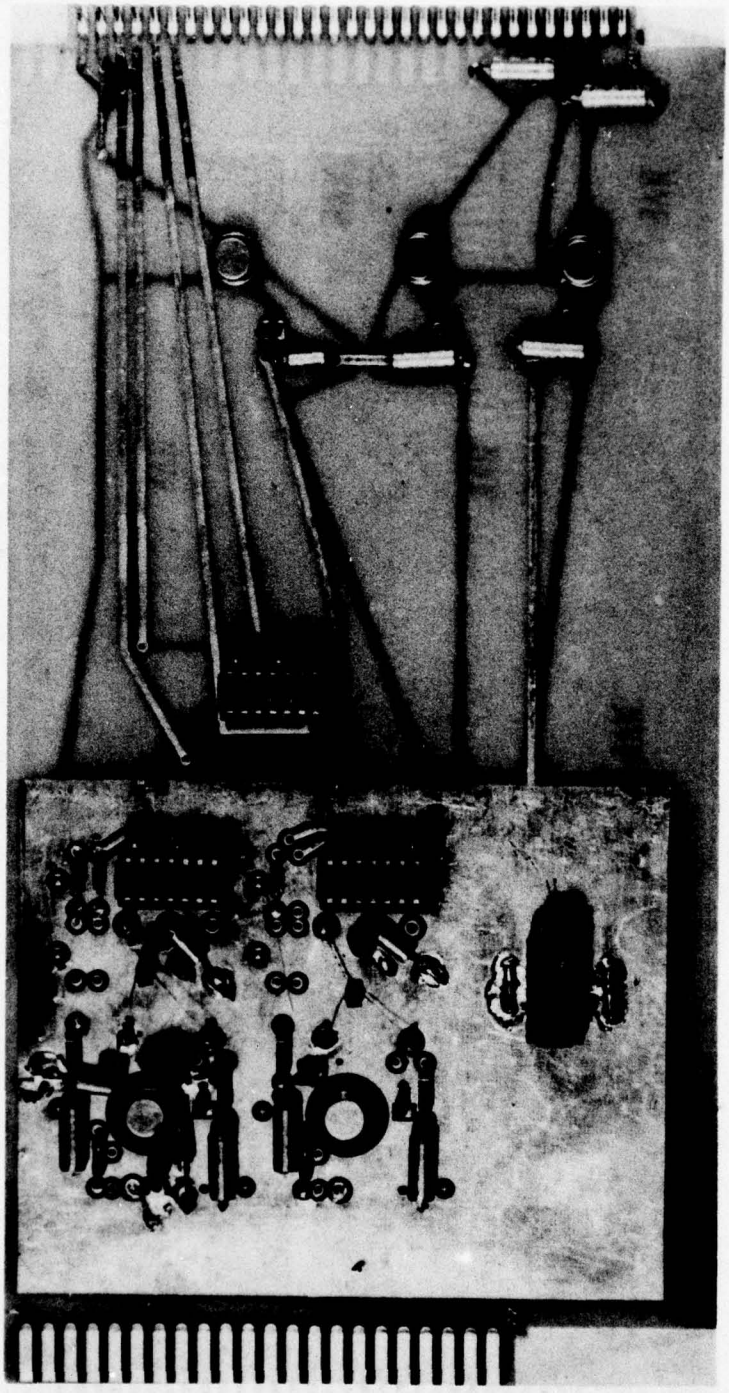

Figure 5. Transmitter board.

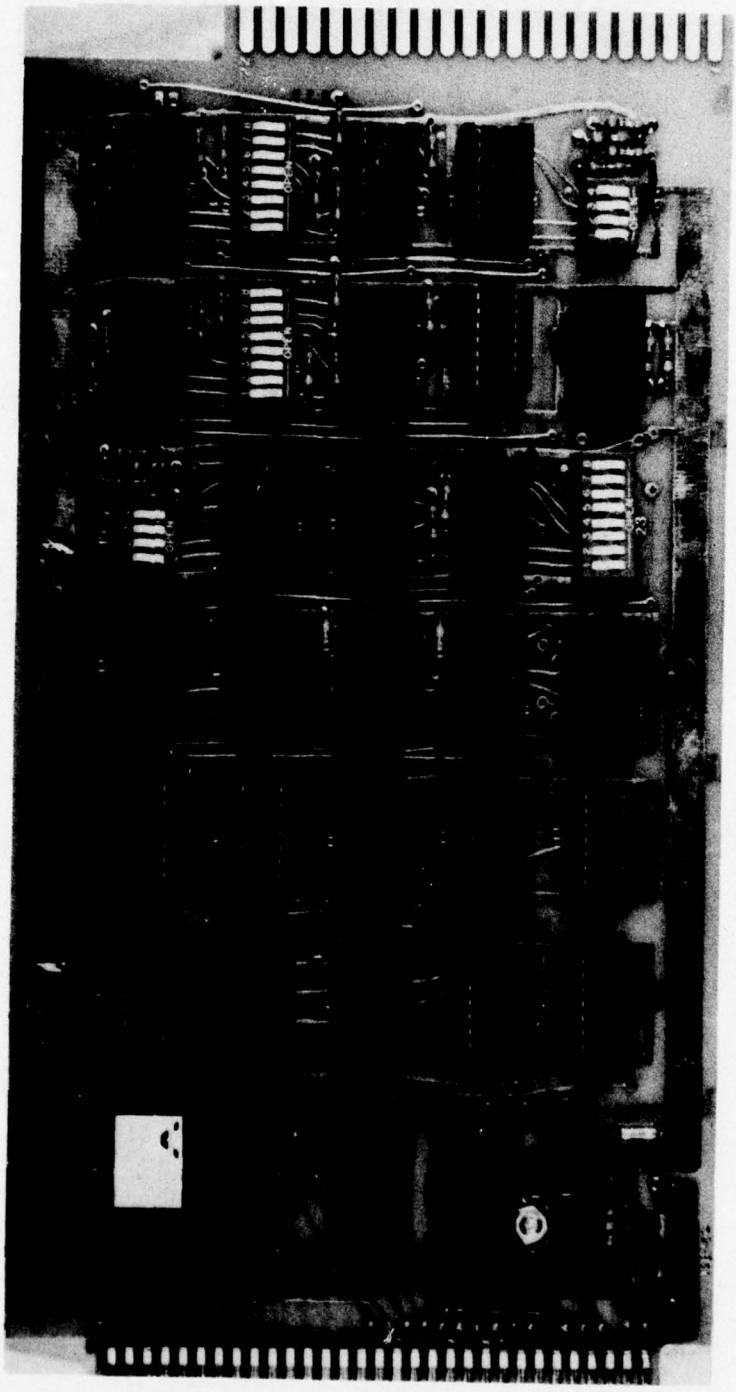

Figure 6. Clock and timing board.

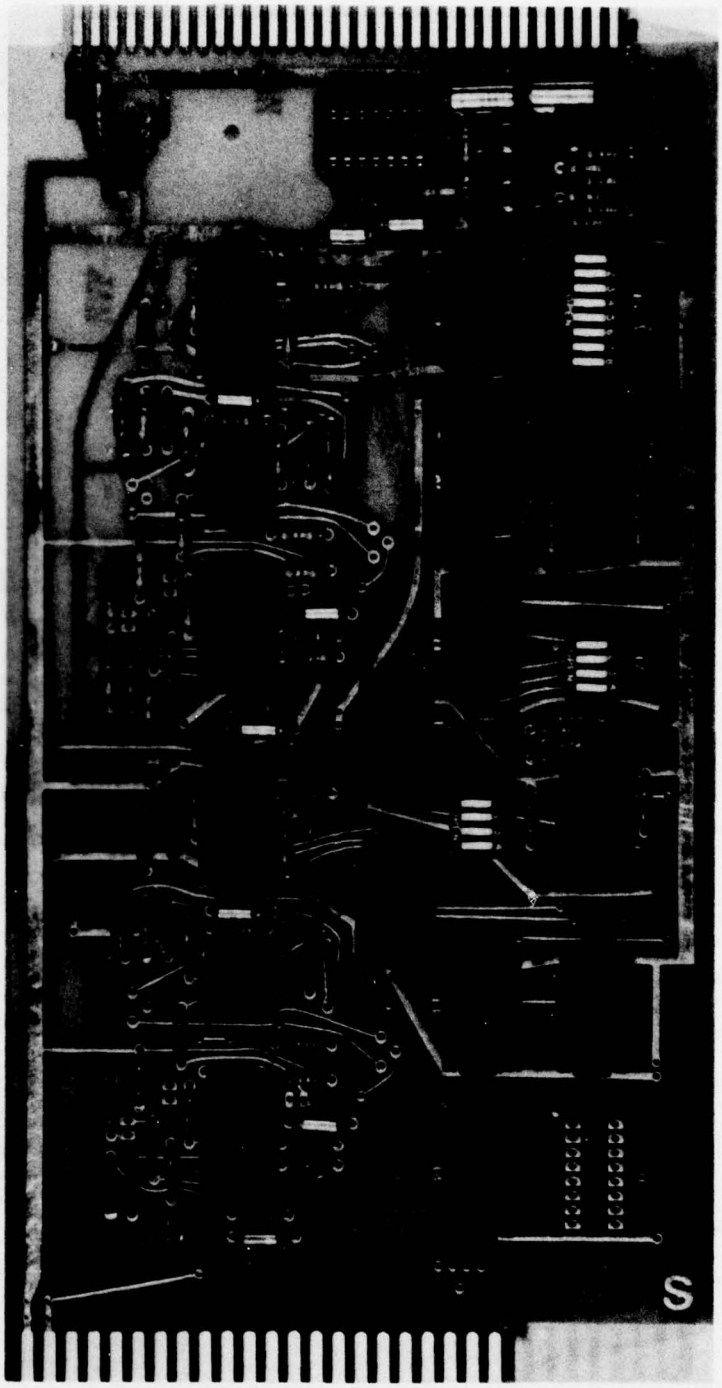

Figure 7. Zero crossing detector board.

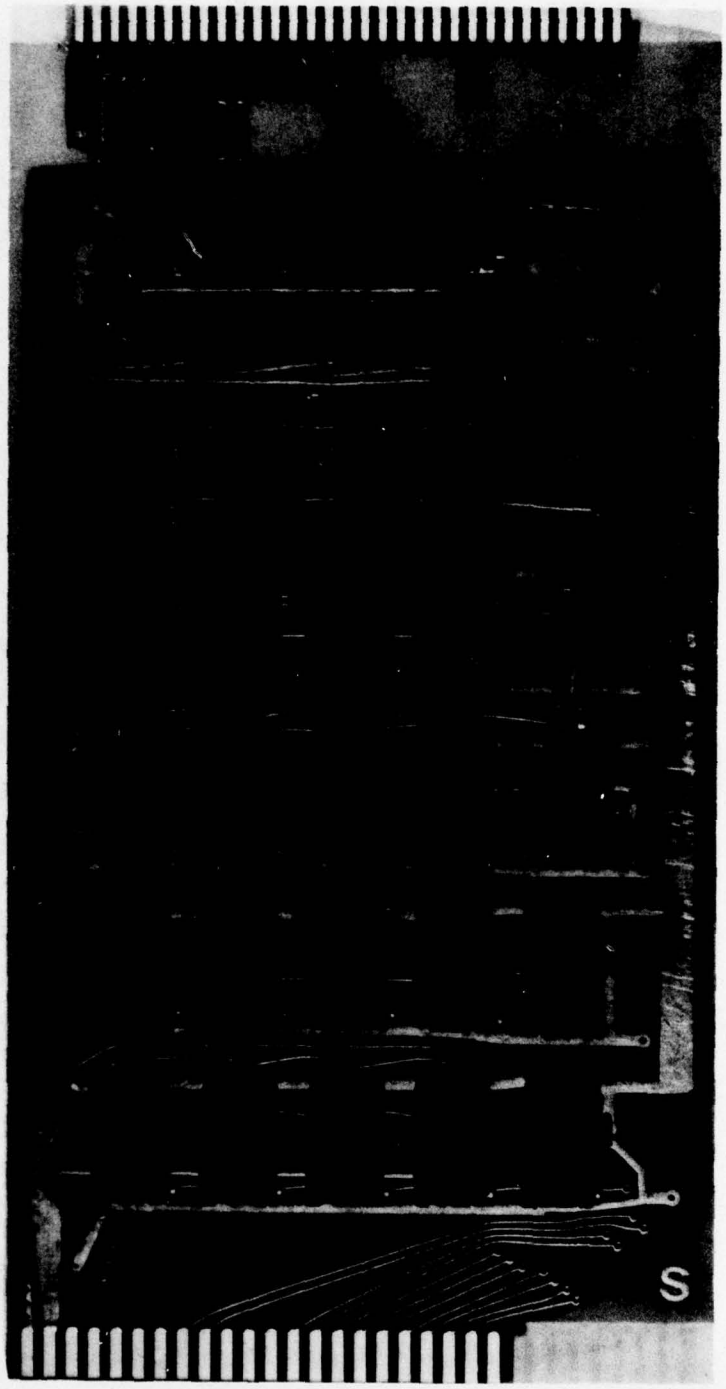

Figure 8. Counter board.

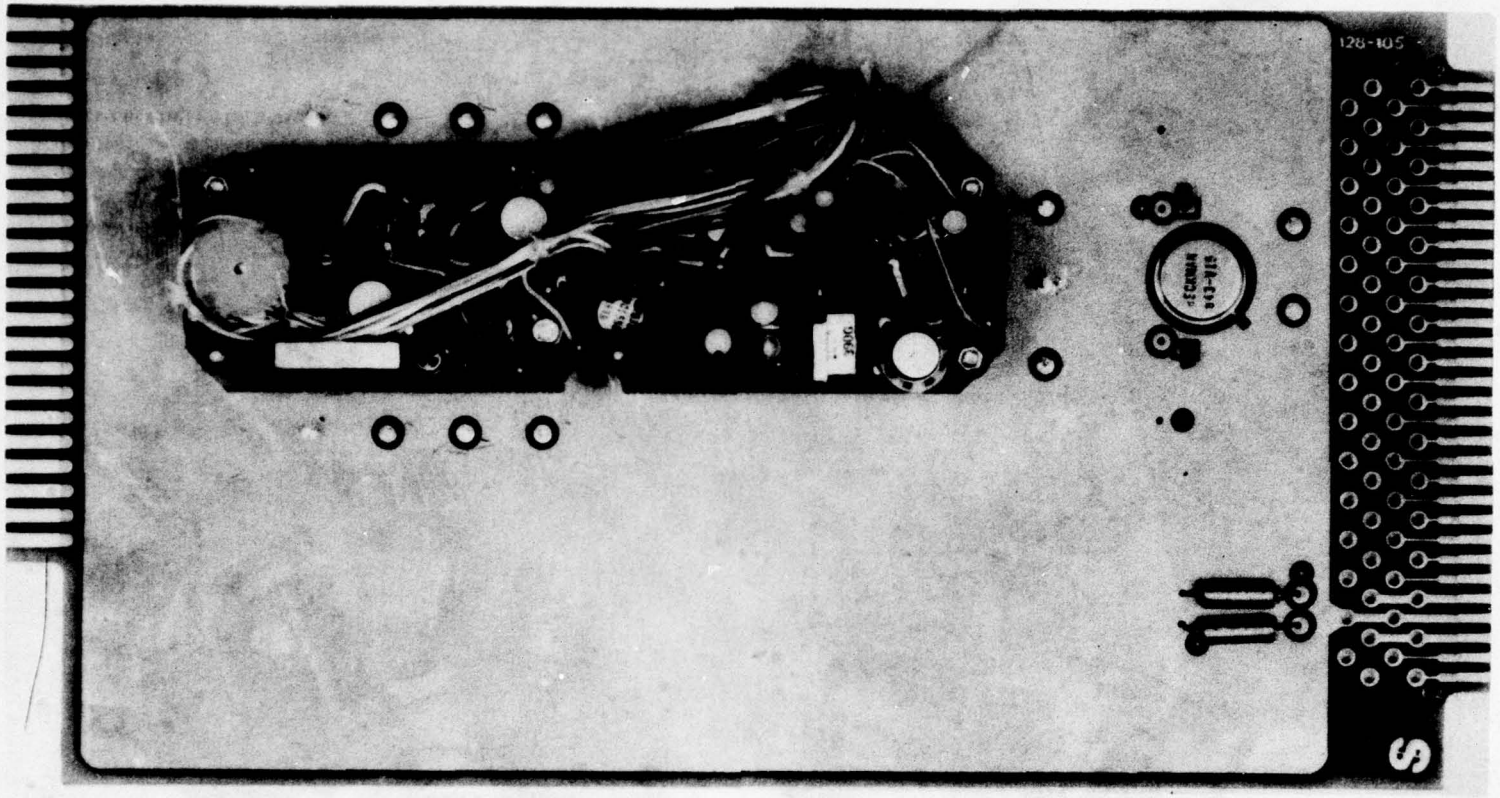

Board fabricated and tested by Simmonds Precision for use in mass flowmeter.

Figure 9. Densitometer circuit board.

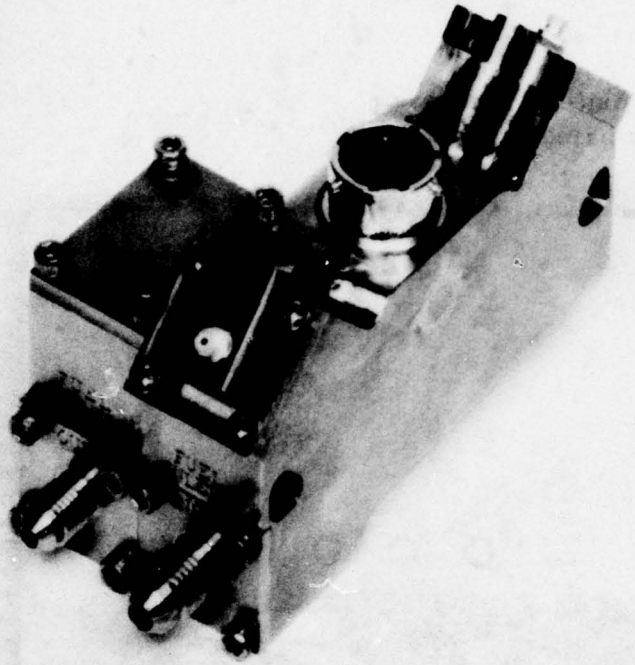

Above: Oblique view shows SS316 cell body; AN-3 and AN-4 fuel outlet and inlet, respectively; multipin electrical connector for ρ and V measurements; μdot connectors for testing ultrasonic transducers and velocimeter.

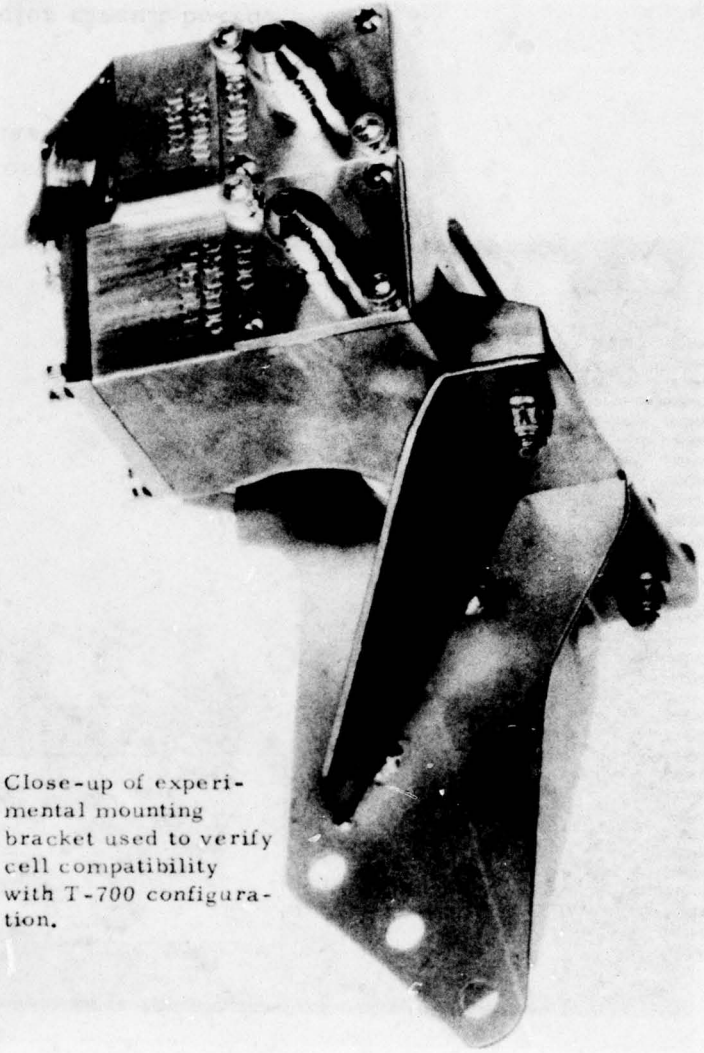

Close-up of experimental mounting bracket used to verify cell compatibility with *T-700 configuration*.

Figure 10. Fuel mass flowmeter cell fabricated of SS 316.

1" = 25.4 mm

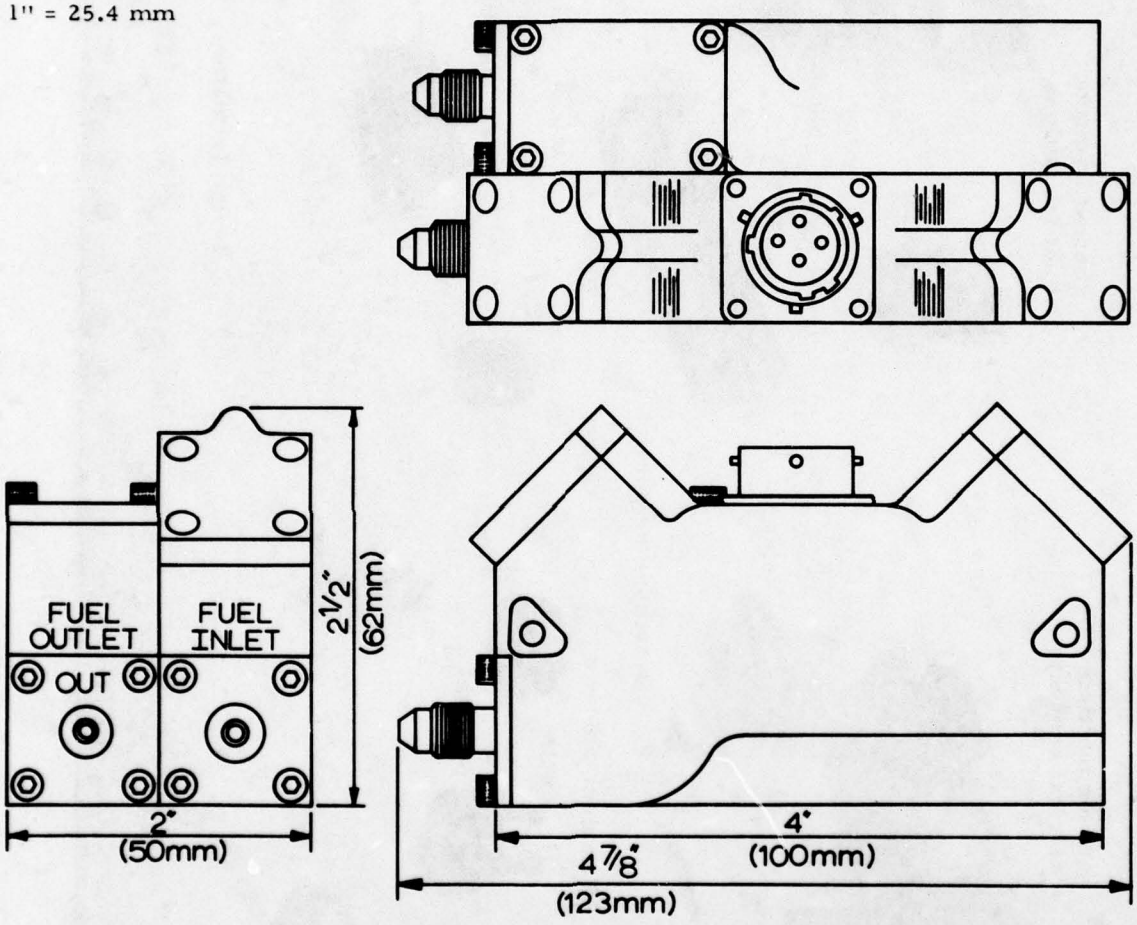

Figure 11. Flow cell outline dimensions.

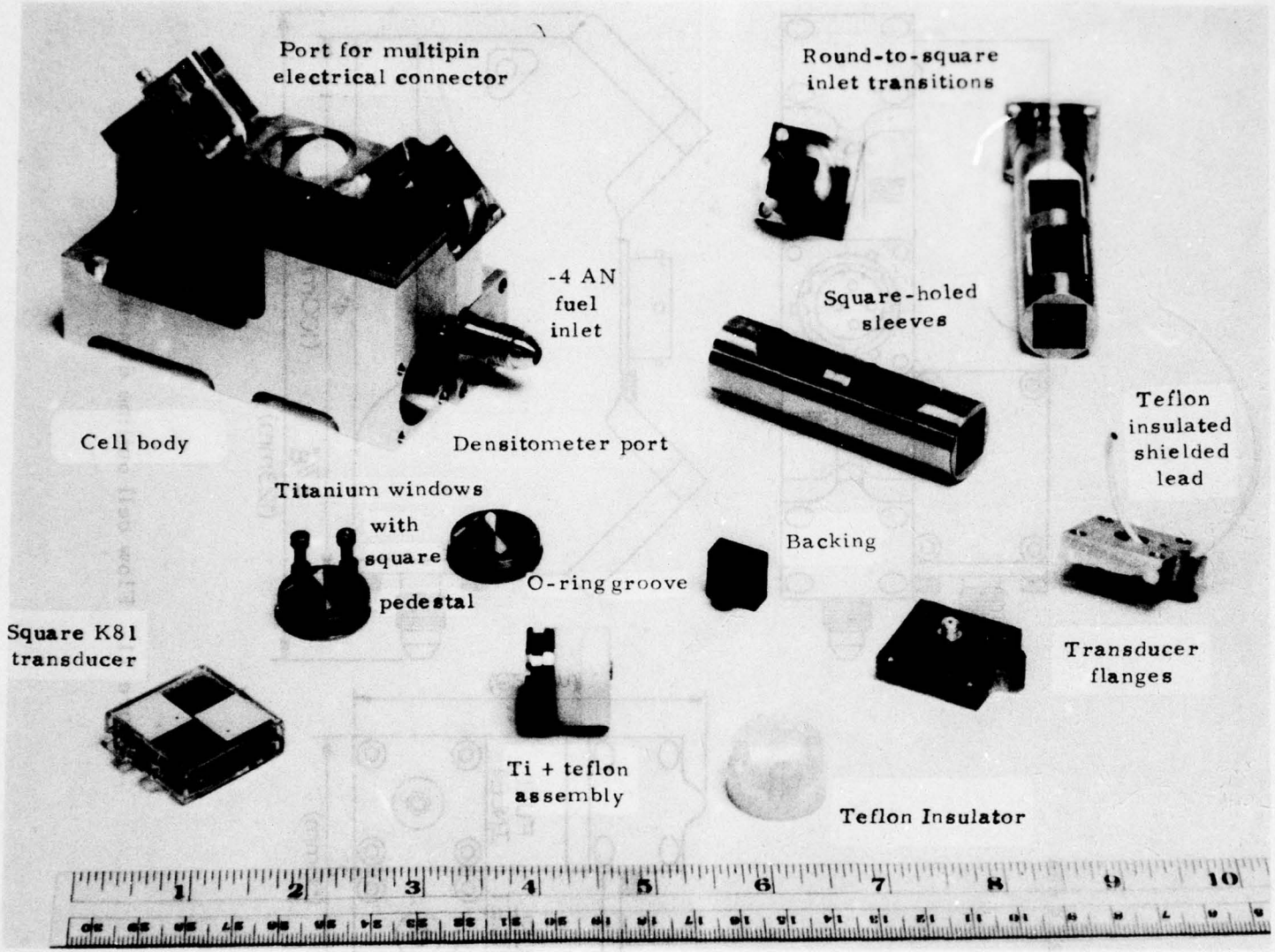

Figure 12. Aluminum flow cell model, and components.

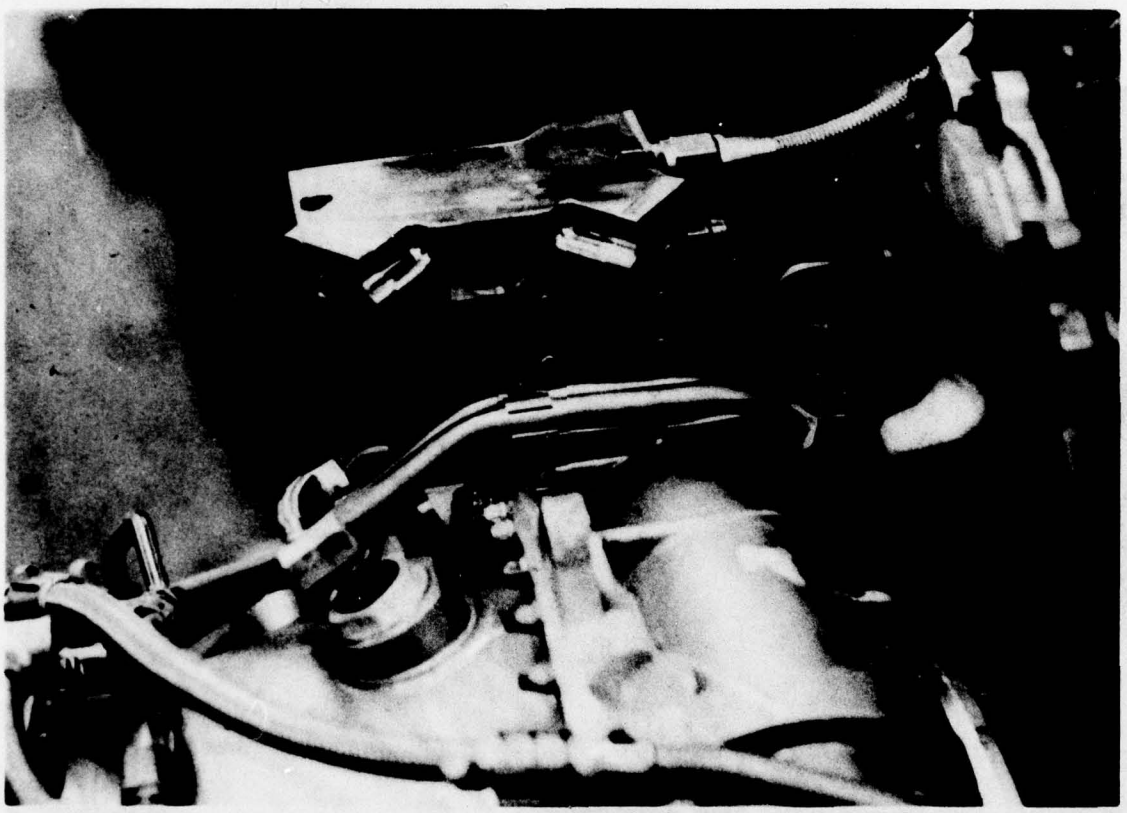

One wiring harness would connect to multipin fitting (not shown here) in circular region between 45° "legs".

Figure 13. Photo of $\dot{M}$ cell mounted on T-700 engine.

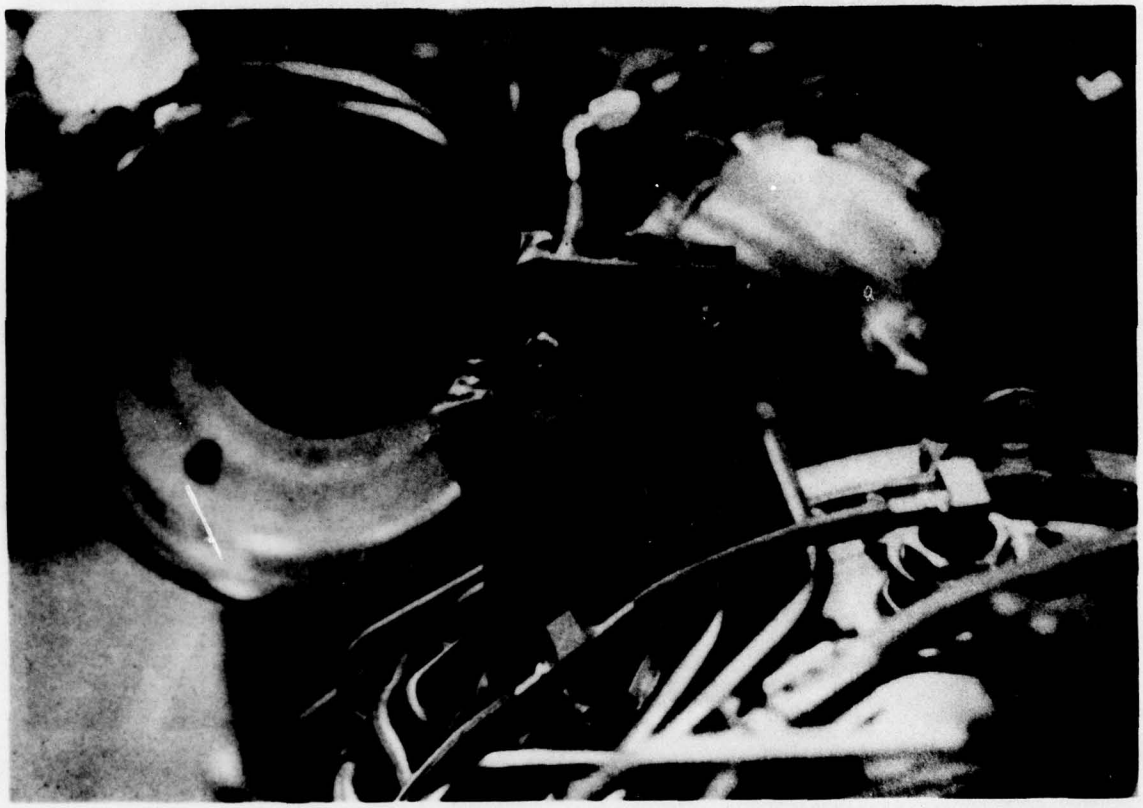

Figure 14. End view of M cell mounted on T-700 engine.

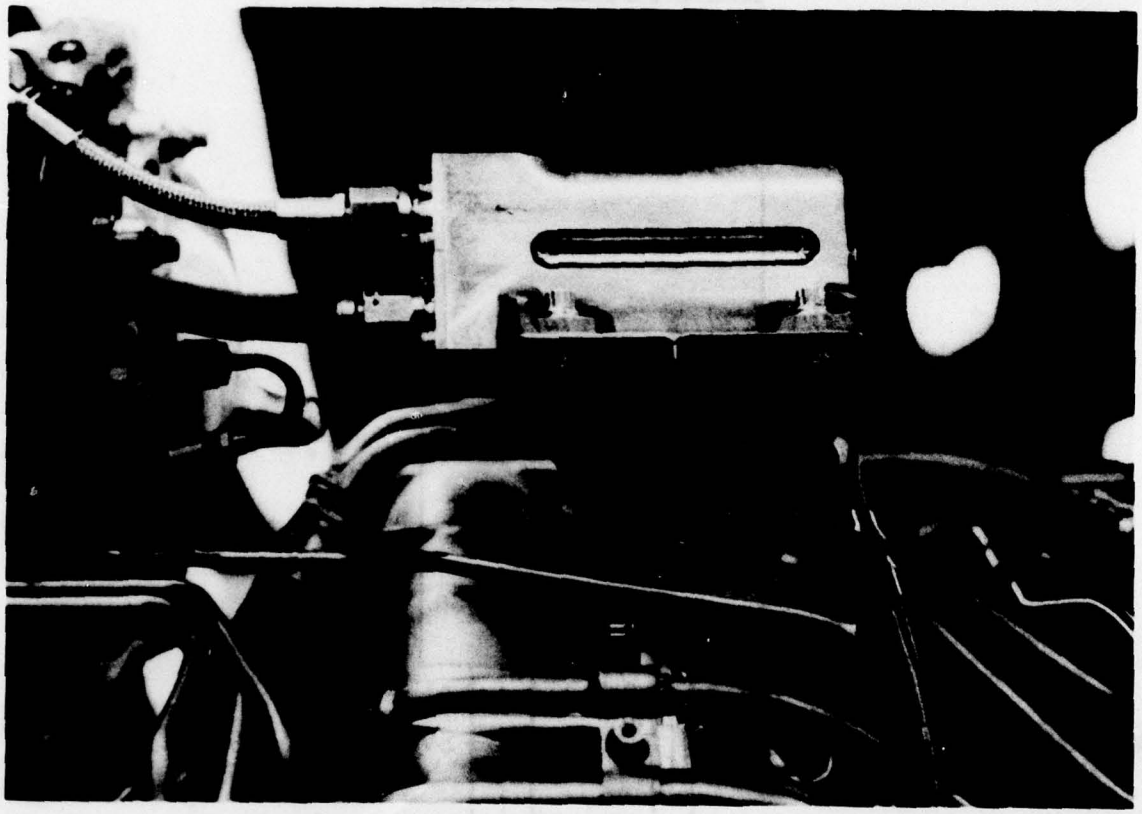

Figure 15. Tilted top view of M cell mounted on T-700 engine.

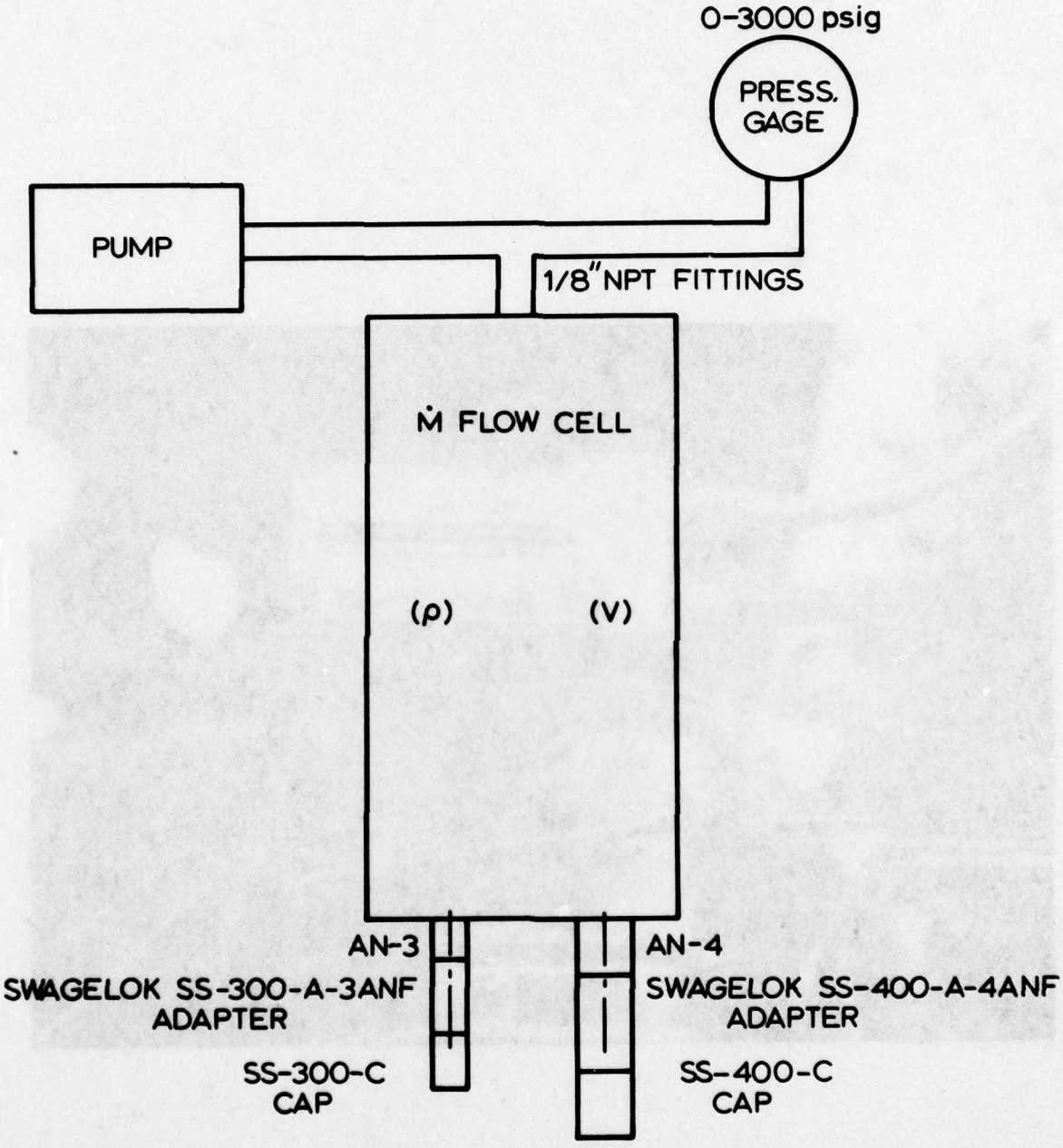

Figure 16. Schematic of hydrostatic pressure test conducted April 1977.

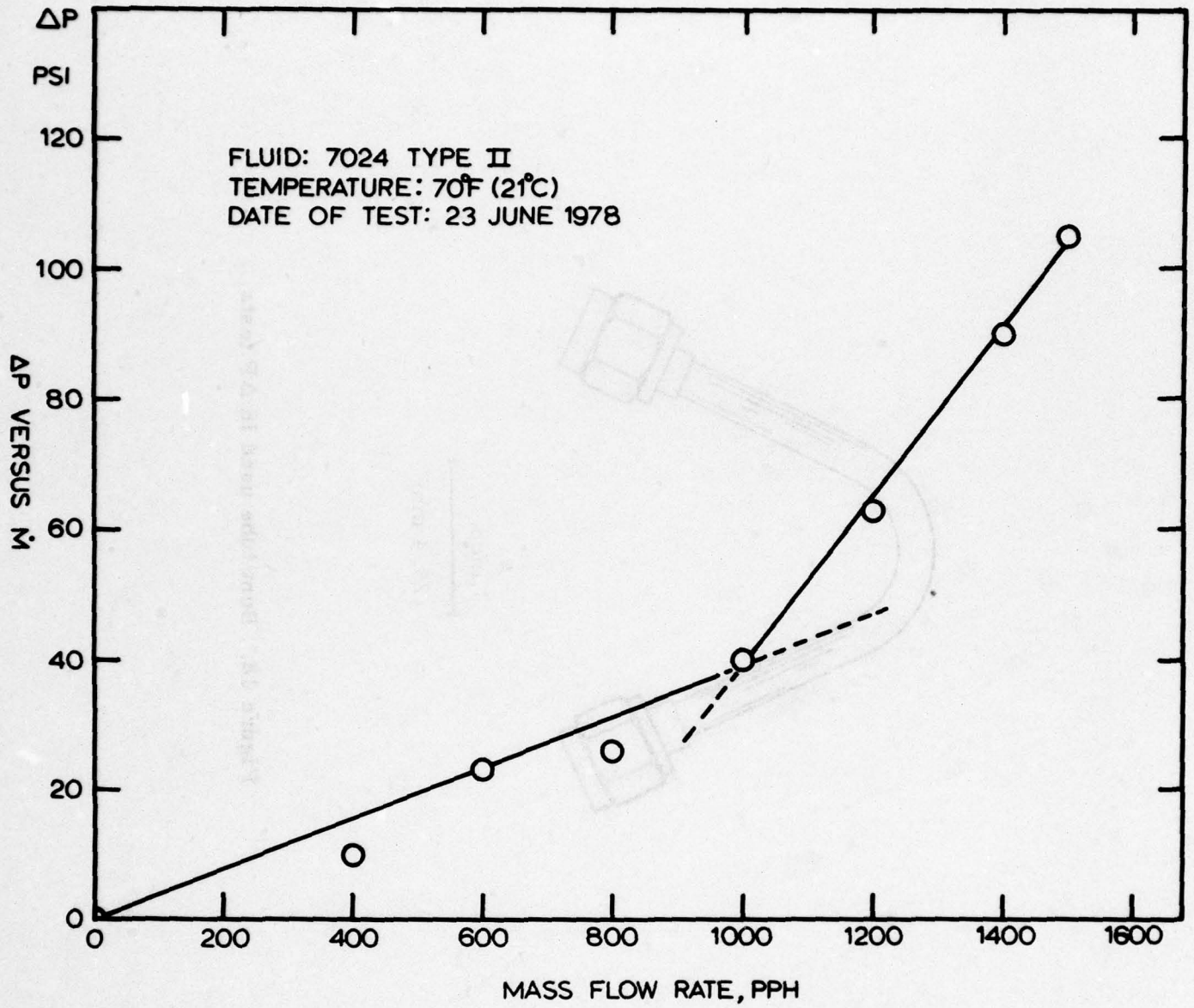

Figure 17. ΔP versus M

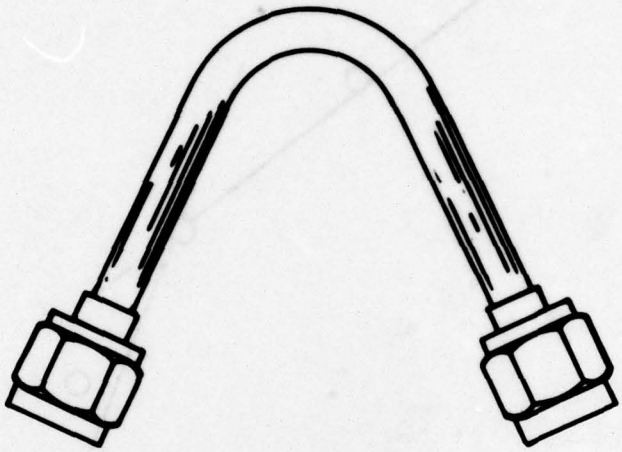

Figure 18. Bent tube used in ΔP tests.

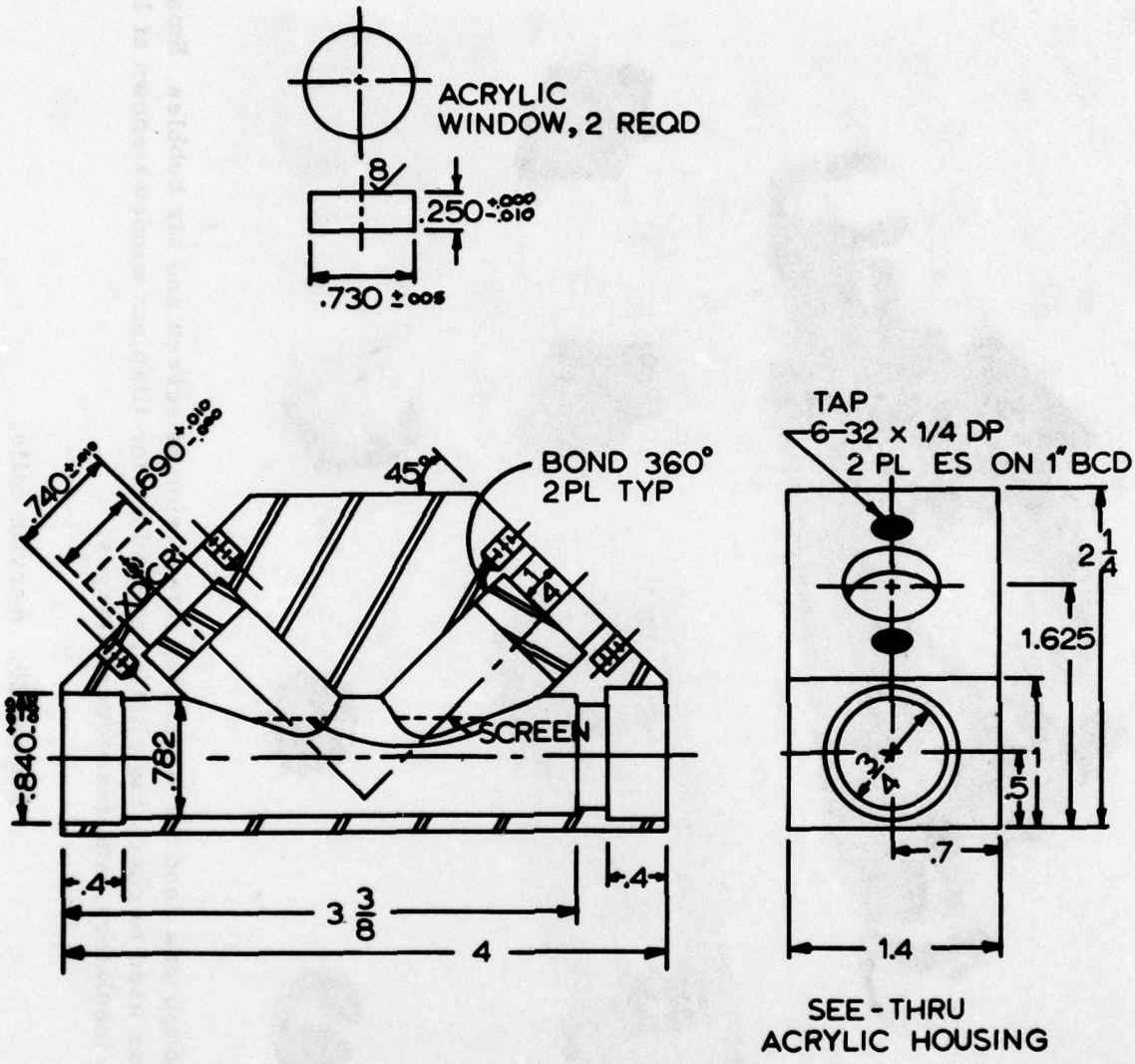

Figure 19. Transparent flow cell to test if screens trap vapor bubbles (e. g., air bubbles in water).

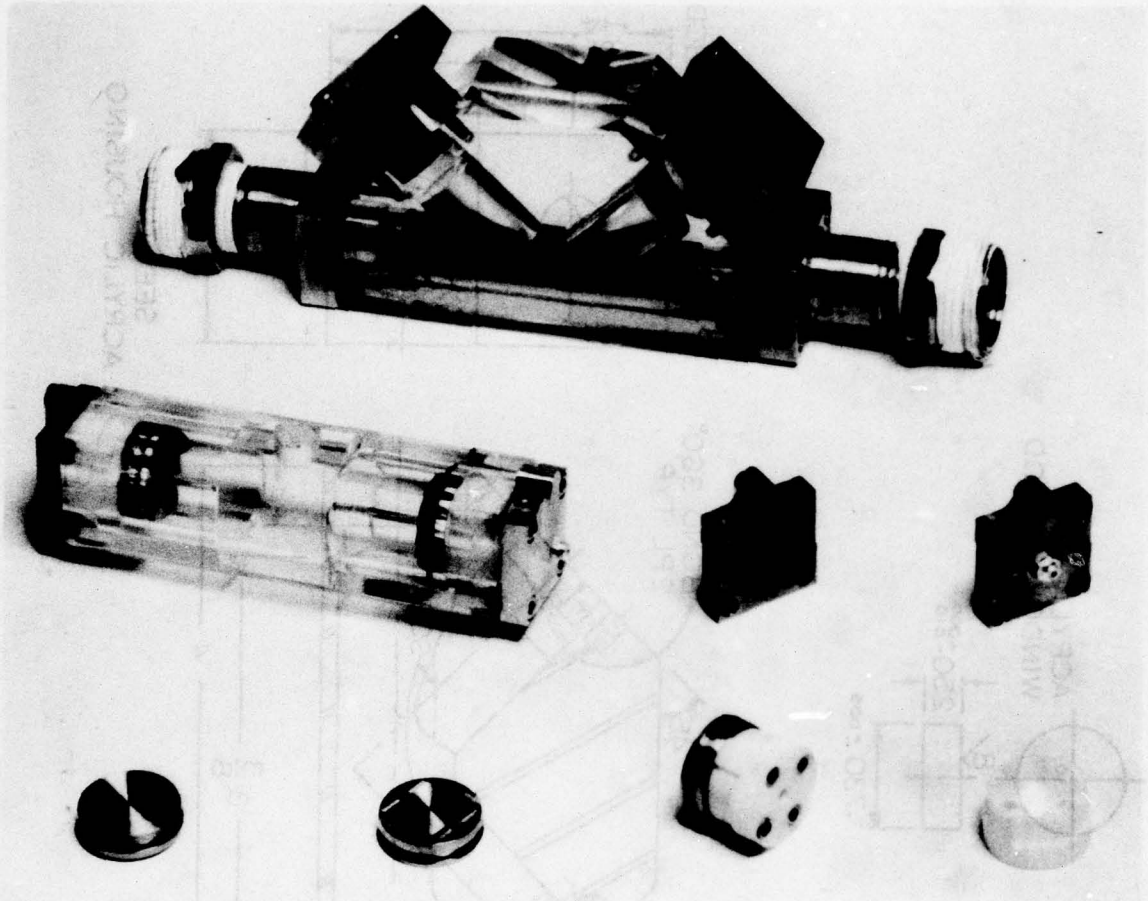

Assembly at top was used for observing interaction of screen and air bubbles. Smaller assembly was used to check installation procedure for titanium windows shown at lower left, Teflon insulators, and transducer flanges.

Figure 20. Acrylic cells.

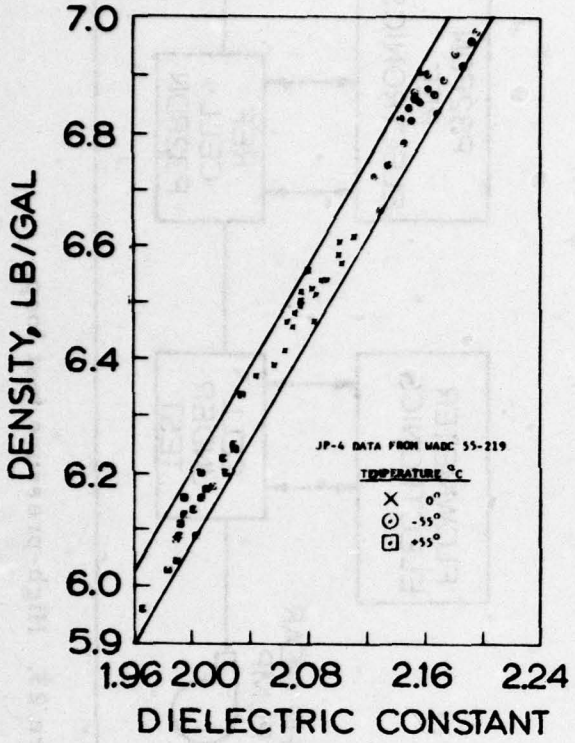

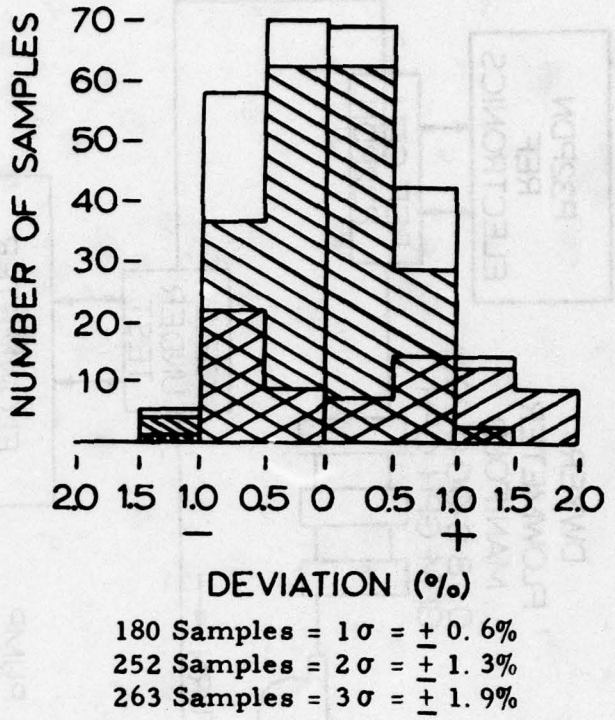

Figure 21. Densitometer calibration from Reference 2.

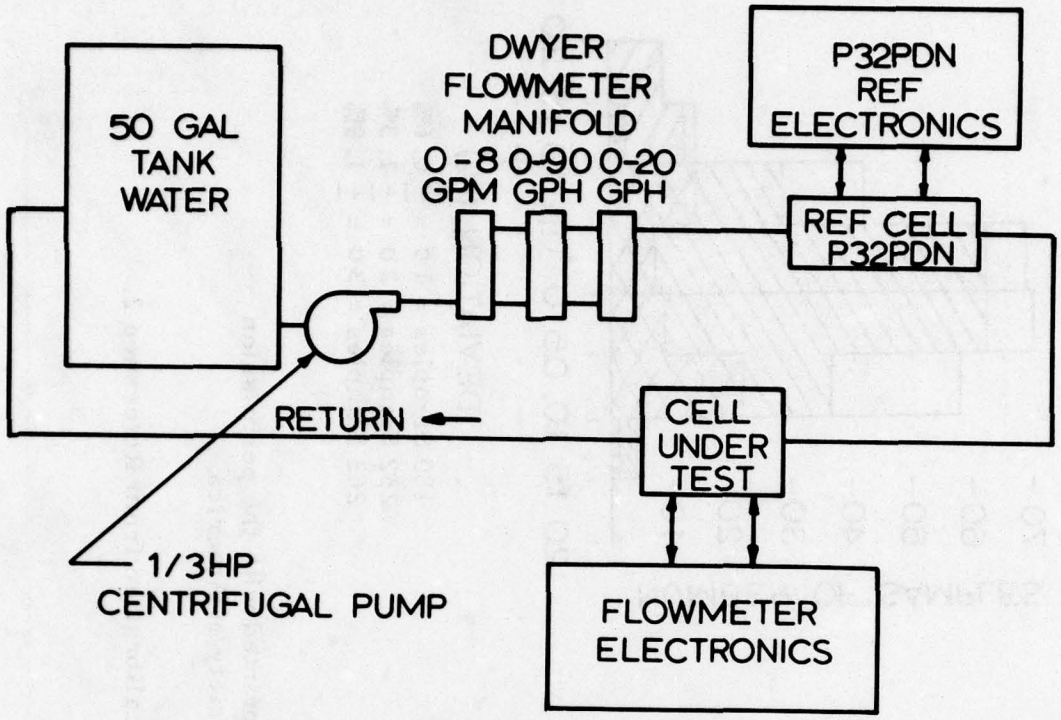

Figure 22. Low-pressure test loop.

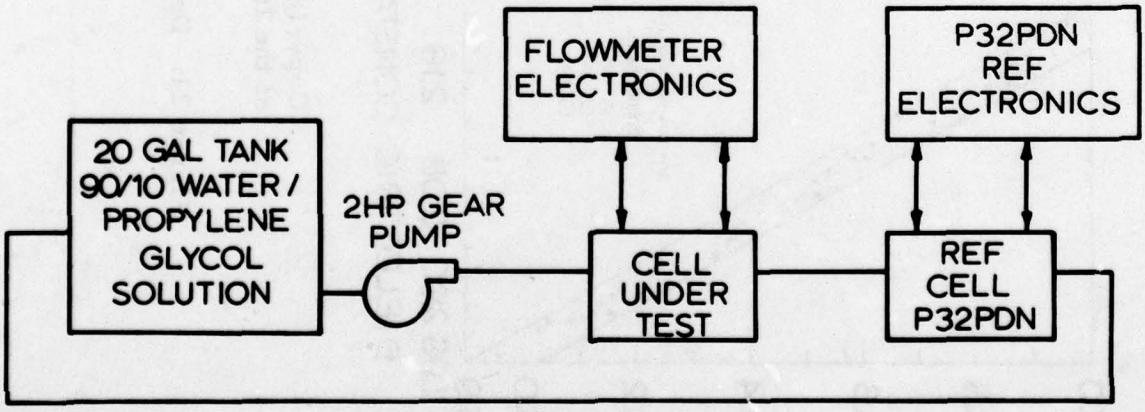

Figure 23. High-pressure test loop.

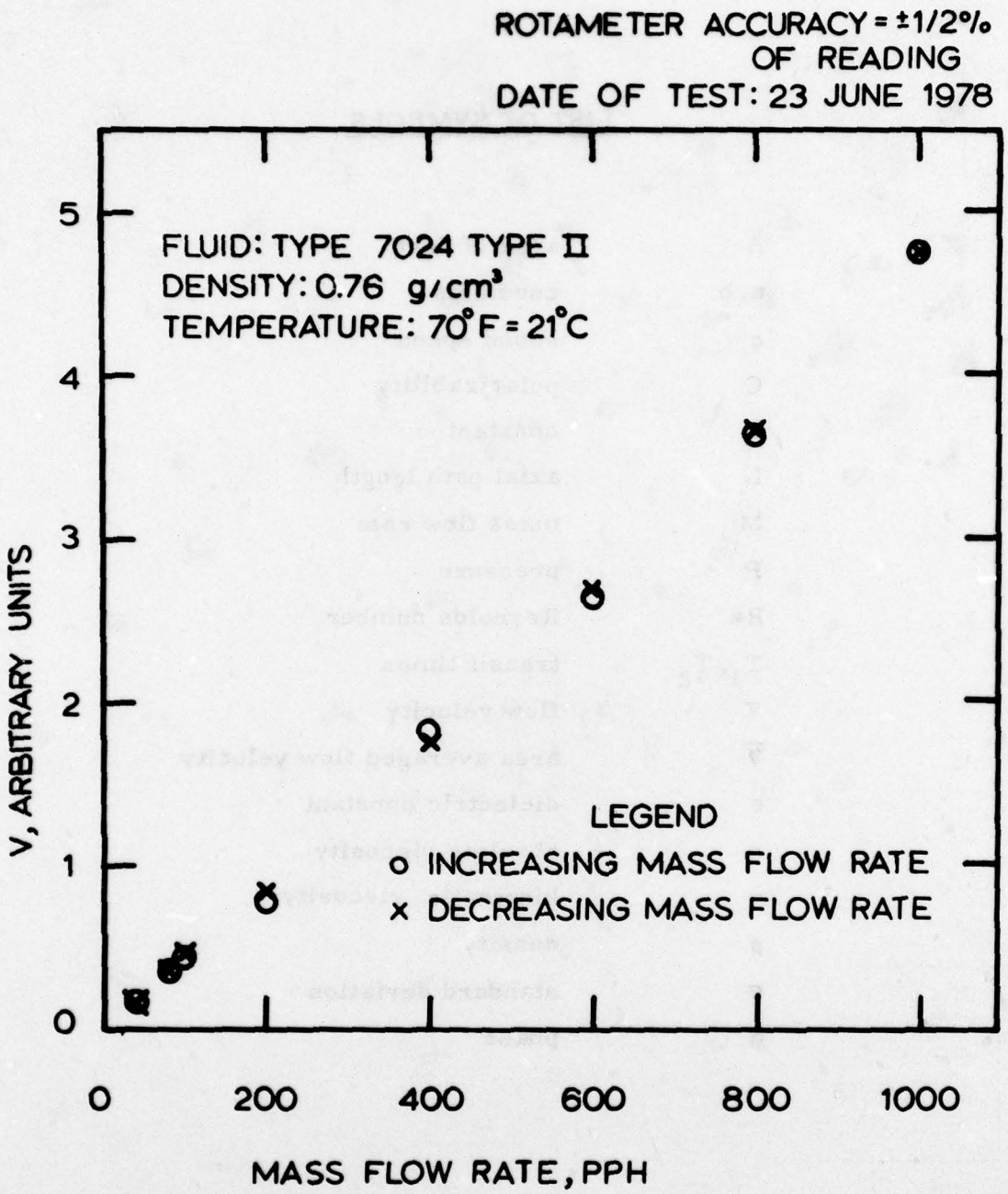

Figure 24. Calibrating fluid test results.

LIST OF SYMBOLS

A	area of duct
a, b	constants
c	sound speed
C	polarizability
k	constant
L	axial path length
$\dot{M}$	mass flow rate
P	pressure
Re	Reynolds number
T_1, T_2	transit times
V	flow velocity
$\overline{V}$	area averaged flow velocity
ϵ	dielectric constant
η	absolute viscosity
ν	kinematic viscosity
ρ	density
σ	standard deviation
ϕ	phase